Polymer Chemistry

Accepted Manuscript

This is an *Accepted Manuscript*, which has been through the Royal Society of Chemistry peer review process and has been accepted for publication.

Accepted Manuscripts are published online shortly after acceptance, before technical editing, formatting and proof reading. Using this free service, authors can make their results available to the community, in citable form, before we publish the edited article. We will replace this *Accepted Manuscript* with the edited and formatted *Advance Article* as soon as it is available.

You can find more information about *Accepted Manuscripts* in the Information for Authors.

Please note that technical editing may introduce minor changes to the text and/or graphics, which may alter content. The journal's standard Terms & Conditions and the Ethical guidelines still apply. In no event shall the Royal Society of Chemistry be held responsible for any errors or omissions in this *Accepted Manuscript* or any consequences arising from the use of any information it contains.

ROYAL SOCIETY OF CHEMISTRY

www.rsc.org/polymers

Solution Processed Thick Film Organic Solar Cells

Chunhui Duan, Fei Huang* and Yong Cao

Institute of Polymer Optoelectronic Materials and Devices, State Key Laboratory of Luminescent Materials and Devices, South China University of Technology, Guangzhou 510640, P. R. China

Email: msfhuang@scut.edu.cn

ABSTRACT: Solution processed bulk-heterojunction (BHJ) organic solar cells (OSCs) are an emerging next-generation photovoltaic technology. Laboratory-scale power conversion efficiencies (PCEs) of OSCs exceeding 10% in single-junction devices and approaching 12% in multijunction devices, respectively, have been achieved. However, the translation of this technology to industrial high throughput manufacturing need the development of practically useful photoactive materials and processing methods that can produce efficient devices with large active layer thickness. In this review, we introduce the factors that determine the optimal thickness of active layer in OSCs at first. The significant advances in materials development and processing methods toward efficient thick film OSCs are summarized subsequently.

KEY WORDS: organic solar cells, bulk-heterojunction, thick film, fill factor, power conversion efficiency

1. Introduction

As a promising sustainable energy technology, organic solar cells (OSCs) attract significant attention from both academic and industrial community over the past two decades owing to its prospect of producing high-efficient, large-scale, and flexible photovoltaic modules via inexpensive roll-to-roll processing or ink-jet printing.[1-5] These devices are a class of thin film solar cells in which the core component—the photovoltaic layer is composed of electron-donors and electron-acceptors. As shown in Fig. 1a, the bulk-heterojunction (BHJ) blend of the donor and acceptor is sandwiched between a transparent conducting electrode and a back reflecting metal electrode.[1] To guarantee Ohmic contact and efficient charge extraction in devices, hole- and electron-collecting layers are usually inserted between the active layer and electrodes. Normally, both semiconducting conjugated polymers and small molecules can be used as electron donors, while fullerene derivatives such as [60]PCBM and [70]PCBM ([6,6]-phenyl-C_n-butyl acid methyl ester, with n = 61 and 71, respectively) are used as electron acceptors. In the past few years, extensive efforts have been devoted to increase the power conversion efficiency (PCE) of OSCs via optimal molecular design and synthesis,[6-14] morphology control and study,[15-19] interface modification,[20, 21], and new device structure design.[22-25] Encouragingly, laboratory-scale PCEs of OSCs exceeding 10% in single junction[26-33] devices and

approaching 12% in multijunction devices,[34, 35] respectively, have been achieved. Moreover, stability test showed that an operation lifetime approaching ten years is possible for OSCs,[36, 37] which suggest the dawning of a new photovoltaic technology. In order to push OSCs forward to a practical technology, however, a lot of technical challenges are yet needed to be overcome. A consensus in OSCs community is that large area manufacturing in combination with high throughput processing such as roll-to-roll methods are at the heart of OSCs in the future. However, the laboratory high PCEs have not been successfully translated to large area devices that are fabricated via roll-to-roll processing. One of the major issues hindering the laboratory-to-industry translation of OSCs is to find the ideal thickness for various layers that best compromises the device performance and processing maneuverability.

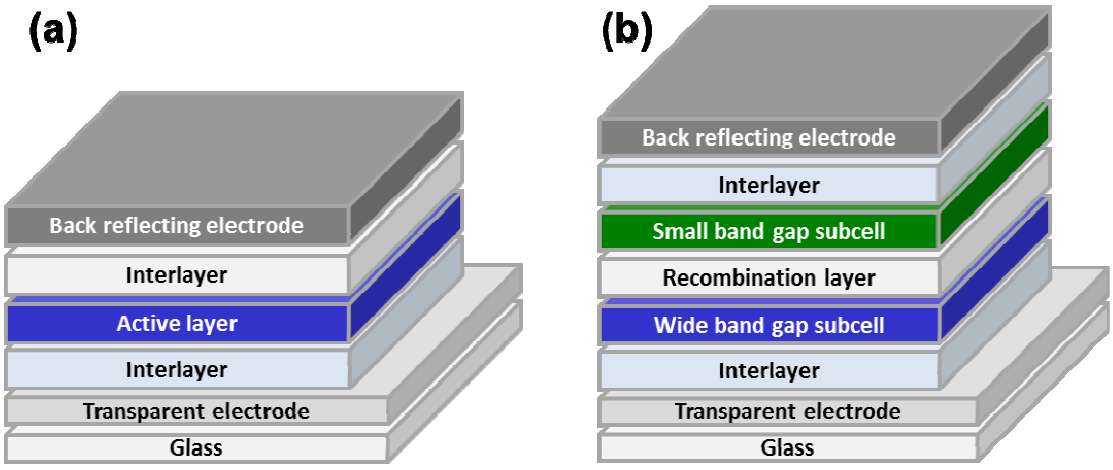

Fig. 1 Device configuration of (a) single junction and (b) double junction tandem organic solar cells.

Currently, most state-of-the-art photoactive materials afford PCE maxima in very

small active layer thickness (80–120 nm).[32, 38-45] Thicker films can absorb incident light more efficiently, but the devices normally delivered a sharp drop in fill factor (FF) and thereby PCE. The active layer thickness restriction causes several issues for high throughput manufacturing of large area OSCs.[46] First, thin layer leads to poor product yields as thin films on rough substrates (e.g. plastic and web) are highly susceptible to point defects, which scale exponentially with area.[47] Secondly, layer thickness restriction results in poor reproducibility as relatively small variation in layer thickness will produce large difference in solar cell performance.[48] Third, thin layer restrict the choices of printing/coating techniques for manufacturing.[49] Obviously, photoactive materials that can afford high efficiencies in a large range of BHJ film thickness are of significant importance for high throughput manufacturing of large area OSCs. On the other hand, OSCs with multijunction structure (Fig. 1b) also need photovoltaic materials that are able to tolerate a broad range of thickness variation.[24, 25, 50] These materials allow freedom in optimizing the optical electric field distribution within multijunction device to balance the performance of the subcells.[51] Up to date, only a few materials can, however, provide high PCEs in BHJ film thickness over 200 nm. Moreover, the guidelines of molecular design and device optimization protocol toward thick BHJ film OSCs are also yet to be established.

Therefore, a review article that summarizes the important achievements in this topic and analyzes the molecular design rationales and processing protocols is highly desired for OSCs community. In this review, we will summarize the important advances in materials development and processing methods of OSCs with thick

photoactive layer. The factors that limit the realization of thick film OSCs will be analyzed at first, and the emphasis will be mainly put on the introduction and analysis of the significant material systems and processing methods that enable efficient thick film devices. We hope this review can provide useful laws for the future design of practically useful photovoltaic active materials and device optimization protocols toward thick film OSCs and further push OSCs forward to succeed as a practical technology.

2. Factors determining the optimal active layer thickness

2.1 Optical interference effect

For a BHJ-type OSCs, an optimal active layer thickness is determined by the balance between charge carrier optically generation rate and extraction efficiency. In any real device, the incident light cannot be 100% absorbed by the photoactive layer due to the scattering and reflecting of the light at the various interfaces inside the devices, as well as the absorption by the photo-inert layers. With the normal active layer thickness of ≈100 nm, 20–40% of the total incident photon flux were wasted, which dictated that the external quantum efficiencies (EQEs) of OSCs hardly exceed 80% even assuming an 100% internal quantum efficiency (IQE). Larger active layer thickness can increase the absorption and result in higher photocurrent potentially. In fact, thicker active layer usually leads to sharp drop in FF, although the short-circuit current density (J_{sc}) might still be high in thick cells due to the field at short circuit is much higher than at maximum power point.[52] In most cases, J_{sc} droped seriously as

well due to severe bimolecular recombination in thick films. Moreover, the optical interference effects further complicate the thickness optimization.[53] As the thickness of the layers in OSCs is usually smaller than the coherence of the light, the interference between the incident light and the reflecting light from the back reflecting electrode render the percentage of light absorbed by the active layer does not increase monotonically with thickness but featured different maxima (Fig. 2).[54, 55] As a result, most BHJ single junction OSCs produce highest PCE values close to the first interference maxima, which is typically at below 100 nm active layer thickness. Taking the achievable IQE of ≥90% as reported in some material systems into account,[38, 51, 56-58] obtaining an 80% EQE normally requires at least 200 nm active layer thickness (around the second interference maxima) for a typical BHJ device with a metal back reflector. Fig. 2 depicts the photon absorption profile of a P3HT:[60]PCBM blend at different layer thickness and the simulated photocurrent generated with the assumptions of various IQEs.[55] It clearly shows the necessity of thick active layer for high achievable EQEs. In case of a semitransparent device such as a subcell in a multijunction solar cell, an even larger active layer thickness is required to absorb the same amount of light.[59]

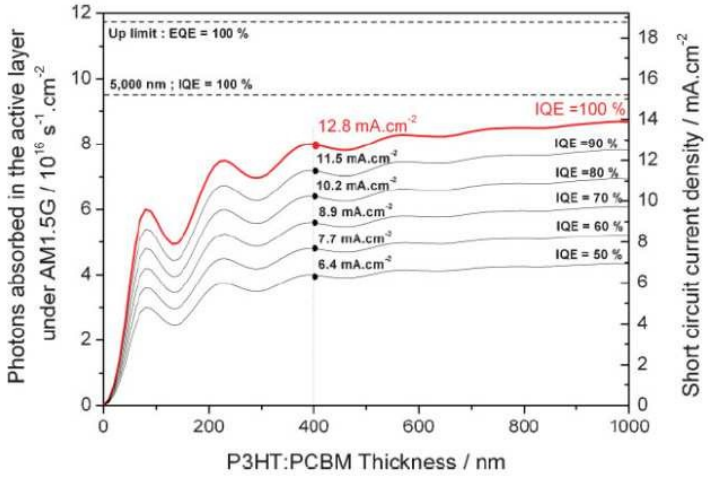

Fig. 2 Number of photon absorbed in the active layer under AM 1.5G caculated by transfer-matrix formalism, for a device having the structur of glass (1 mm)/ITO (140 nm)/PEDOT:PSS (50 nm)/P3HT:[60]PCBM (x nm)/Al (100 nm). The right axis represents the corresponding short-circuit current density at various IQE, indicated in the graph. Produced with permission from ref. 55, Copyright 2009, John Wiley & Sons. Inc.

2.2 Space-charge effect

As mentioned above, increasing active layer thickness is, however, accompanied by the drastic degradation of FF in most cases, which overcompensates the gain in absorption and thereby leads to decline in overall PCE. Under higher thickness, the photo-generated charge carriers in active layer must travel with a longer distance before being collected at electrodes. Moreover, a thicker layer decreases the magnitude of the built-in electric field across the device, which further prolongs the transport of the charge carriers before reaching electrodes and increases the loss of non-geminate recombination.[59] In addition, the structural defects of organic

semiconductors which is known as unintentional doping,[52, 60-62] and the space charge created by the lower carrier in a device with imbalanced charge carrier mobility will result in the formation of field-free region.[52, 59, 63] In OSCs, the transport of free charge carriers before being collected at respective contacts rely on drift and/or diffusion.[59] The free charge carriers are transported via drift under the assist of built-in electric field, and transported via much lower process of diffusion under field-free region. As a result, the photo-generated charge carriers in this electric-free region will experience significant bimolecular recombination and contribute little to the photocurrent. Kirchartz et al.[52] analyzed the space-charge effect in a series of poly[(4,4'-bis(2-ethylhexyl)dithieno[3,2-*b*:2',3'-*d*]silole)-2,6-diyl-*alt*-(4,7-bis(2-thienyl)-2,1,3-benzothiadiazole-5,5'-diyl)] (Si-PCPDTBT):[70]PCBM[64, 65] solar cells with different layer thicknesses via drift-diffusion simulation, a method which is widely used to study the charge carrier transport and collection process in OSCs,[52, 59, 63, 66-69] by considering the case of unintentional *p*-doping or mobility asymmetry. The simulation results show that in thin solar cells close to the first interference maximum the space-charge effect is minor with the whole active layer is under depletion region (Fig. 3a and 3c). But in thick solar cells around the second interference maxima the space-charge has a significant effect on device performance with a large portion of active layer under field-free region (Fig. 3b and 3d). As the charge carrier collection efficiency is only high in the depletion region, the thick cells around the second interference maxima have a substantially reduced collection either close to the back contact in case of *p*-doping or close to the front contact in case of mobility asymmetry

(electron mobility ≫ hole mobility).

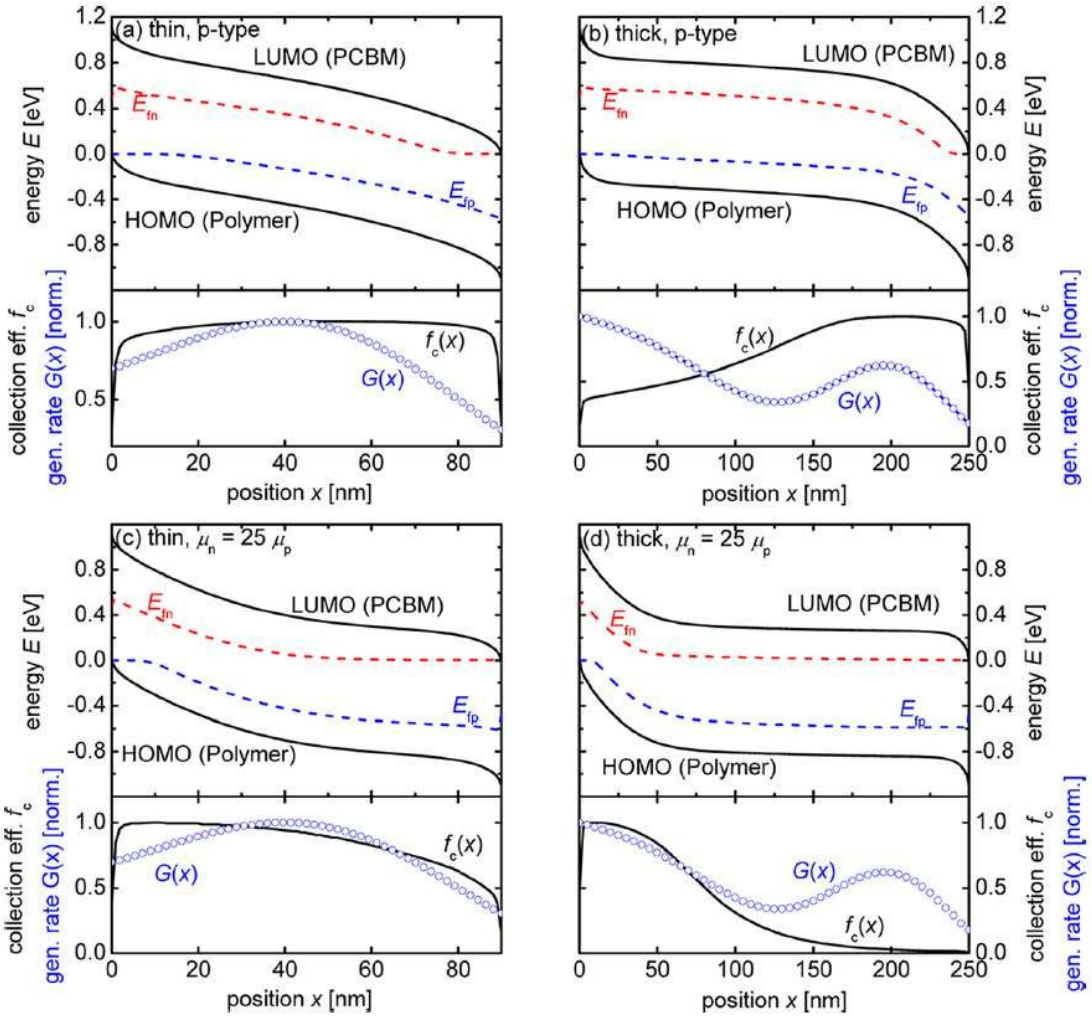

Fig. 3 (a-d) Band diagrams of (a, c) a 90 nm thin solar cell with (a) p-type doping or (c) asymmetric mobilities at short circuit and one sun illumination compared with the analogous band diagrams of (b, d) a 250 nm thick solar cell. The collection efficiency plots show that in thick cells the collection efficiency is only high in the depletion region, which means that the thick cells with a significant space-charge effect caused by doping or mobility symmetry have a drastically reduced collection either close to the back contact (p-doping) or close to the front contact (electron mobility ≫ hole mobility). Produced with permission from ref. 52, Copyright 2012, American Chemical Society.

2.3 Charge carrier mobility requirements

At this point, sufficient high mobilities and balanced transport are thus required for efficient charge carrier collection to produce high FF in OSCs especially for thick devices,[46, 59, 70] although in thin devices imbalanced mobilities can produce high FF if both hole mobility and electron mobility are high enough in some cases.[71] It is worth pointing out at first that vertical charge carrier mobilities that are measured by fitting the space-charge-limited current (SCLC) acquired form diodes can more accurately evaluate the charge transport ability than the mobilities measured in field-effect transistors (FETs).[5] Very recently, Bartelt et al.[59] systematically studied the mobility requirements for obtaining high FF in various active layer thickness by using one-dimensional drift-diffusion simulations based on poly(3-hexylthiophene) (P3HT):[60]PCBM system. The simulation results disclosed that the FF of the BHJ solar cells decreases significantly with increasing thickness at low hole mobility but can keep flatten once the SCLC hole mobility of the P3HT:[60]PCBM blend increased up to 10^{-2} cm^2 V^{-1} s^{-1} (Figure 4a and 4b). This hole mobility threshold is also required to obtain a 0.8 FF at 300 nm active layer thickness. For achieving a FF of 0.65 with the active layer thickness of 300 nm, a SCLC hole mobility of 10^{-3} cm^{-2} V^{-1} s^{-1} is required. Given the fact that electron mobility in BHJ solar cells can be relatively high ($\approx 5 \times 10^{-3}$ cm^{-2} V^{-1} s^{-1} measured by SCLC)[72-74] and hole is usually the slower carrier in real devices, the efforts should be placed on increasing the hole

mobility of the electron donors in OSCs. Furthermore, the drift-diffusion simulation indicates that the required charge carrier mobility under balanced transport is dependent on the recombination rate constant.[59] As shown in Figure 4c, reducing the recombination rate constant of OSCs would significantly reduce the required charge carrier mobility for high FF. In this term, further research is also needed to disclose the factors that affect recombination rate constant and to provide clues on how one can reduce recombination.

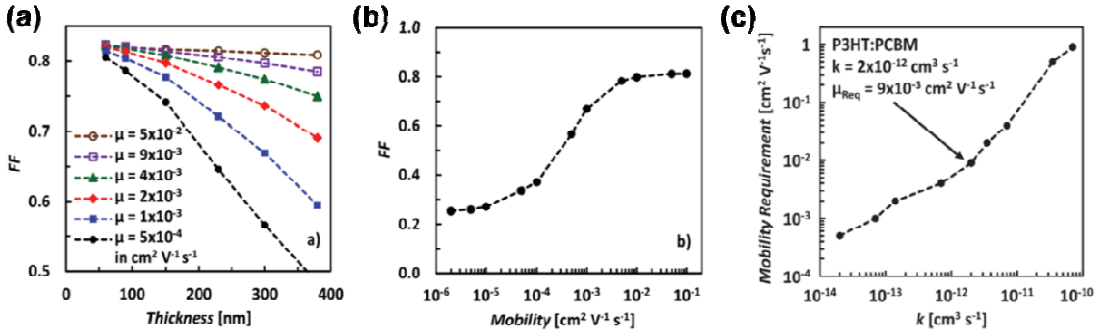

Fig. 4 (a) Fill factor as a function of active layer thickness for simulated P3HT:[60]PCBM solar cells with equal hole and electron mobilities and recombination rate constant of 2×10^{-12} cm^3 s^{-1}. (b) Fill factor as a function of charge-carrier mobility for simulated P3HT:[60]PCBM solar cells with equal hole and electron mobilities and recombination rate constant of 2×10^{-12} cm^3 s^{-1}. (c) Charge-carrier mobility (balanced) required to achieve a 0.8 fill factor in a 300 nm thick simulated P3HT:[60]PCBM solar cell as a function of recombination rate constant, *k*. Produced with permission from ref. 59, Copyright 2015, John Wiley & Sons. Inc.

A statistical analysis on mobility guidelines for high FF in small molecule BHJ solar cells was conducted by Nguyen's group[70] with experimentally measured SCLC

mobilities and the corresponding solar cell FFs based on eleven solution processable small molecules. The data suggests that in order to achieve high FF (>0.65) in small molecular BHJ solar cells, both hole and electron mobilities must be greater than 10^{-4} cm^{-2} V^{-1} s^{-1}. Achieving such high mobilities was found to be more important to high FF than establishing hole and electron mobilities that were balanced but less than 10^{-4} cm^{-2} V^{-1} s^{-1}. It is worth pointing out that this mobility threshold was established on small molecular solar cells with thin active layer. Moreover, they proposed that neat film mobility measurements is an useful tool for screening potential materials intended for high FF small molecular BHJ solar cells as neat film hole mobility values for a given molecule were generally found to set the upper limit of blend film hole mobilities. Noticeably, the mobility threshold set by Nguyen's group is much (1~2 order of magnitude) smaller than that set by McGehee's group. This difference may be caused by the different analysis methods and different material systems. For both polymer and small molecular BHJ solar cells, it was found that hole is most often the slower carrier in real devices, the simulation and analysis provided by the two groups may have implications for the development of new polymers and electron accepting materials for efficient thick film OSCs.[59, 70]

2.4 Film microstructure and BHJ morphology

It is well known that the J_{sc} and FF of OSCs are dominated by film microstructure and morphology of BHJ blend, which are inclusive of a lot of structural information. In thin-film OSCs, bicontinuous interpenetrating network with optimal domain size have

proved to be critical to efficient charge generation, efficient charge transport and suppressed bimolecular recombination.[15-17] Compared to thin-film (≈100 nm) devices, thick-film OSCs put forward more requirements for BHJ morphology. Crystallinity and the degree of molecular ordering, oriention of conjugated backbone with respect to substrate, molecular orientation at donor/acceptor interface, domain size and purity, mix phase, and vertical phase separation are all required to be exquisitely controlled. It is well known that PTB7-type polymers have been the best donor polymers in BHJ OSCs in the past few years, because it can form a "near optimum" BHJ morphology in thin film.[11, 38, 75, 76] However, it was revealed that PTB7 features relatively low molecular ordering, impure polymer domains, and relatively low hole mobilitie.[77] These explain why there is no report on efficient PTB7-based thick-film solar cells.

However, it is highly challenging to optimize all the aforementioned metrics at the same time. For example, high crystallinity and high degree of molecular ordering are beneficial for charge transport, but the increase of crystallinity comes often at the expensing of increasing the domain size because of fast and strong aggregation of molecules during film drying or even in solution state.[78] High crystallinity is also favorable to obtain high domain purity. Significant impure donor phases can lead to serious bimolecular recombination, which aggravates with the increase of active layer thickness.[79] Encouragingly, the effective control of crystallinity, domain size, and domain purity was recently demonstrated by Yan's group[27] benefitting from the temperature-dependent aggregation behavior of conjugated polymers via rational polymer design. The backbone orientation with respect to substrate is a critical

metric that dictates the charge transport in BHJ solar cells.[17, 80] Face-on backbone orientation is superior to edge-on orientation due to the hopping mechanisms of charge transport in organic semiconductors. The structure of conjugated backbone and the pattern of alkyl chains are both found to affect backbone orientation. However, there are still lack of effective and universal means to control backbone orientation.[80]

Due to the higher surface energy of fullerene than conjugated polymers, graded distribution of the ingredient of donor/acceptor blend, which is known as vertical phase gradation, is usually observed in BHJ systems.[81-83] The enrichment of fullerene in the bottom of active layer is beneficial to hole transport and collection in OSCs with inverted device configuration but it is opposite in conventional devices.[82] The treatment of wet films that contain residues of high boiling point solvent additives with nonsovent have proved to be effective methods to optimize the vertical phase gradation in conventional OSCs.[84, 85] However, the methods to control vertical phase gradation in BHJ films without using high boiling point solvent additives are yet needed to be developed.

Comprehensively introduction of film microstructure and morphology control, and the influence of various morphological characteristics on the performance of OSCs are out of the scope this review. For more knowledge on the topic of morphology of bulk-herojunction OSCs, the reader is encouraged to read other extensive reviews.[15-17] In the following, we will introduce the influence of film microstructure and BHJ morphology on the performance of thick-film OSCs in specific cases.

3. Representative material systems

Up to date, a few semiconducting conjugated polymers afford efficient BHJ solar cells with active layer thickness over 200 nm. In addition to the well-known polythiophenes, a handful of donor–acceptor (D–A) type conjugated polymers also show appreciable device performance at relative high active layer thickness. In this section, we will comprehensively introduce these state-of-the-art material systems according to the type of conjugated framework. More importantly, molecular design strategies and morphology control protocols toward thick film BHJ solar cells will also be discussed based on these materials.

3.1 Polythiophenes

P3HT (P1 in Scheme 1) is the most-studied conjugated polymer in OSCs due to its low-cost synthesis and reproducible device performance in different laboratories.[86] The photovoltaic performance of P3HT:[60]PCBM based solar cells are insensitive to the thickness variation in a range from 100 to 300 nm.[87-89] Coincidently, most reports on large area OSC modules use P3HT:[60]PCBM as the active layer, probably for this exact reason.[46] It was reported that a 520 nm thick P3HT:[60]PCBM device shows similar or even slightly better overall performance than the 170 nm device without sacrificing FF.[90] However, further increasing the thickness leads to significant reduction in device performance. Zeng et al.[91] disclosed that thermal annealing can help to recover the performance of thick-film device. Impressively, a high FF of 0.64 was observed in a 1200 nm thick device after annealing at 110 °C for 20 minutes. This

recovery was attributed to the formation of favorable vertical phase separation in thick P3HT:PCBM film via thermal annealing. By replacing [60]PCBM to indene-C_{60} bisadduct (ICBA), an acceptor possessing higher-lying lowest unoccupied molecular orbital (LUMO), the resulting P3HT:ICBA solar cells can also work well at a relative high active layer thickness of ≈200 nm. High PCEs of ≈7.5% with remarkable FF of ≈0.75 were independently achieved in two research groups.[92, 93] The device parameters of several representative P3HT-based thick-film solar cells are summarized in Table 1. The appreciable FF values are attributable to the relative high hole mobility of P3HT and the preferred morphology in BHJ films. Typical hole mobility of P3HT is around 5×10^{-3} cm^{-2} V^{-1} s^{-1} in single-carrier devices.[73] One of the main drawbacks of P3HT is the low V_{oc} in devices as a result of its high-lying highest occupied molecular orbital (HOMO) level. Recently, Hou's group[94] developed a new polymer P2 with electron-withdrawing carboxylate substituents attached to the side chain to reduce the frontier orbital energy levels. Impressively, P2 demonstrated low sensitiveness to the active layer thickness variation in BHJ devices. The solar cells produce PCE of 7.2% and 6.6%, along with relevant FF of 0.72 and 0.66 at active layer thickness of 94 nm and 230 nm, respectively. However, no mobility data was provided for P2. The same research group further corroborated the effectiveness of varying the active layer thickness of front cell to achieve high performance tandem OSCs benefiting from the relative low thickness sensitivity of P2.[95] The J_{sc} and PCE increased from 7.5 mA cm^{-2} and 8.6% to 11.7 mA cm^{-2} and 10.2%, respectively, when the thickness of P2:[70]PCBM based front cell increased from 72 nm to 210 nm.

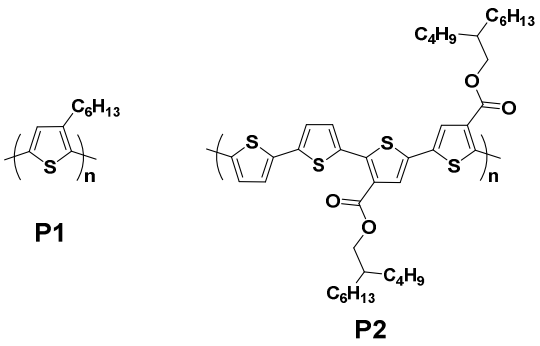

Scheme 1 The chemical structures of P1 and P2.

Table 1 Device performances of polythiophenes-based BHJ solar cells at different active layer thickness.

Polymer,acceptor	*d* (nm)	V_{oc} (V)	J_{sc} (mAcm^{-2})	FF (-)	PCE (%)	Ref.
P1, [60]PCBM	520	0.58	11.5	0.55	3.7	90
P1, [60]PCBM	1200	0.50	9.2	0.64	2.3	91
P1, ICBA	200	0.87	11.4	0.75	7.4	92
P1, ICBA	180	0.89	11.7	0.73	7.5	93
P2, [70]PCBM	94	0.91	11.0	0.72	7.2	94
P2, [70]PCBM	230	0.91	10.6	0.66	6.4	94

3.2 Fluorine substituted polymers

It is well known that fluorination can increase the V_{oc} of the BHJ solar cells due to the deeper HOMO energy levels of the fluorinated polymers via the electron-withdrawing effect upon fluorination.[96, 97] The improvement in other photovoltaic parameters such as FF and J_{sc} upon fluorination are also often observed although the mechanisms are yet to be fully understood. Several explanations including hole mobility enhancements due to planarization of the backbone and improved intermolecular

order via weak noncovalent interactions (C–H···F, S···F, etc.),[98-100] preferential orientation of the backbone with respect to the discrete D/A interface,[101] favorable π–π stacking orientation of the polymer chain with respective to the substrate[74], and reduced non-geminate and geminate recombination[102] have been proposed.

Benefitting from these special fluorine effects, donor-acceptor type conjugated polymers with fluorine substituents on the periphery of the conjugated back thus constitute the most famous polymer family that can tolerate thickness variation of active layer in BHJ solar cells. The chemical structures of these polymers are exhibited in Scheme 2. The device parameters of the BHJ solar cells are summarized in Table 2. Price et al.[103] created a fluorinated polymer P3 which incorporate benzodithiophene (BDT) as the donor unit and fluorinated benzotriazole (BTA) as the acceptor unit. P3 shows an optical band gap (E_g) of 2.0 eV, which is slightly larger than that of P3HT (1.9 eV). The solar cell made of P3:[60]PCBM shows a high PCE of 7.1% with a notably FF of 0.73 at 250 nm active layer thickness. Moreover, P3-based BHJ solar cells yield a PCE of 6.1% at the active layer thickness of 1 μm. In contrast, the fluorine-free analog of P3 only produce a PCE of 4.3% and a FF of 0.55 at 230 nm layer thickness. The outstanding photovoltaic properties of P3 at large active layer thicknesses were attributed to the high hole mobility of 1.0×10^{-3} cm^{-2} V^{-1} s^{-1}, which is measured in hole-only diodes and is at the same order of magnitude as P3HT blends under the similar conditions.[73] It is discovered that the excellent photovoltaic properties shown by P3 at thick film can only be obtained with polymers of a quite narrow range of molecular weight (≈40 kg mol^{-1}). Both lower and higher

molecular weight lead to significant reduction in FF and J_{sc}.[104] More recently, Li et al.[105] further investigated the influence of fluorine content in a series of BDT-BTA based polymers on the charge carrier mobility and device performance of BHJ solar cells with thick active layer. It is observed that the hole mobility of the polymers, and the PCE and FF of solar cells monotonically increased as increasing fluorine content (Fig. 5). Such enhancements were disclosed to be linked with the improved polymer molecular ordering and preferential face-on orientation of polymer backbone toward the substrate, which are beneficial to charge transport and suppressing charge recombination. More interestingly, OSCs based on P3 with active layer thickness of 250 nm perform well in a wide range of morphologies. The FF above 65% can be kept even with factor of two changes in domain size and factor of two changes in relative domain purity.[106] Min et al.[107] reported a structurally related wide band gap polymer (P4) in which the BDT unit with a thiophene-conjugated side chain was used as the donor unit to form the two-dimensional conjugated structure. P4 affords FF of 0.67 and PCE of 6.0% at 190 nm active layer thickness in P4:[70]PCBM solar cells, but further increasing the thickness to 400 nm leads to a dropped FF of 0.58 and a PCE of 4.7%. The hole mobility of neat P4 film measured in FETs is 2.4×10^{-3} cm^{-2} V^{-1} s^{-1}. Li et al.[108] reported a donor-acceptor polymer made up of dialkylthiol-substituted BDT and monofluorinated benzotriazole, P5, of which the neat film shows a hole mobility 4.3×10^{-3} cm^{-2} V^{-1} s^{-1} of in single-carrier devices. The BHJ solar cells of P5:[70]PCBM generates a high PCE of 7.7% with a FF of 0.71 at 250 nm active layer thickness. Yan's group[109] developed a donor-acceptor conjugated

polymer P6 based on quarterthiophene and fluorinated BTA. P6 enables OSCs with a high PCE of 7.5% and a FF of 0.69 at the active layer thickness of 250 nm. An important structural feature of P6 is the fluorination both on BTA and the central bithiophene units, that introduce strong interchain aggregation for the polymer in solution and highly crystalline polymer film. Moreover, the P6:fullerene blend exhibits a reasonably small polymer domain size.

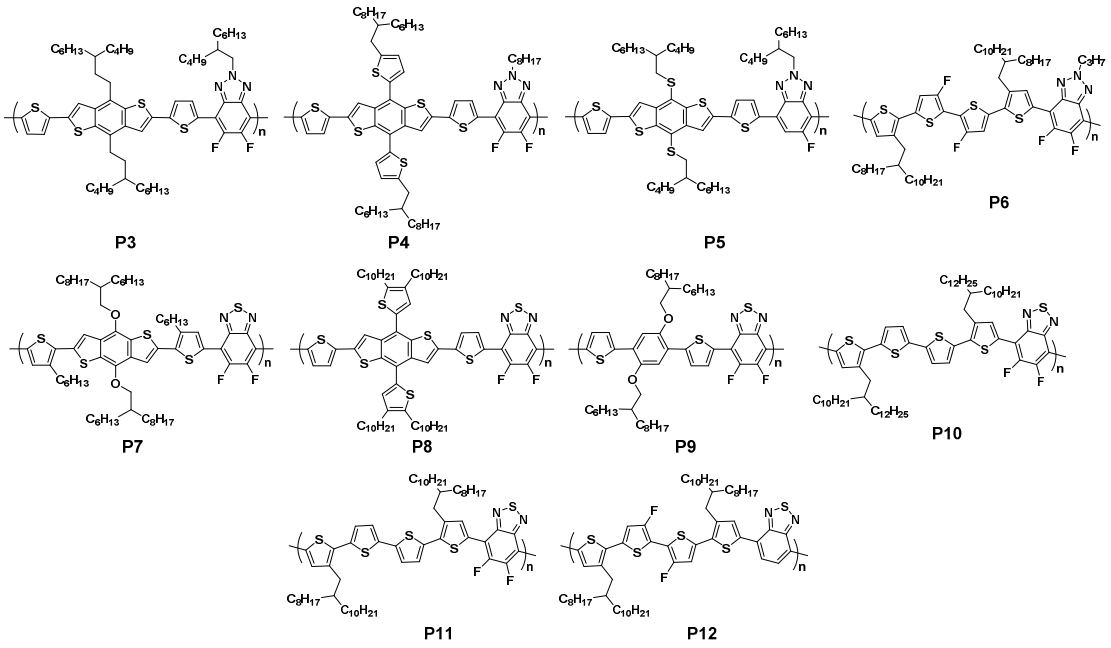

Scheme 2 The chemical structures of fluorinated polymers that allow making efficient thick-film solar cells.

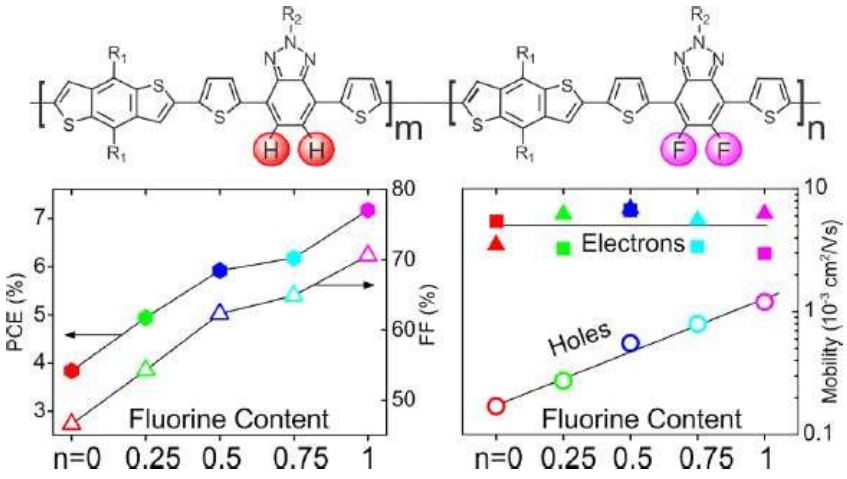

Fig. 5 Power conversion efficiency, fill factor, and charge carrier mobilitis as a function of fluorine content in a series of BDT-BTA polymers. Produced with permission from ref. 105, Copyright 2014, American Chemical Society.

Table 2 BHJ solar cell performances of fluorinated polymers that allow making efficient thick-film solar cells.

Polymer, acceptor	d (nm)	V_{oc} (V)	J_{sc} (mAcm^{-2})	FF (-)	PCE (%)	μ_h (cm^2 V^{-1} s^{-1})	μ_e (cm^2 V^{-1} s^{-1})	Ref.
P3, [60]PCBM	250	0.79	11.8	0.73	7.1	1.0×10^{-3} [a]	-	103
P3, [60]PCBM	1000	0.74	14.0	0.54	6.1	1.0×10^{-3} [a]	-	103
P4, [70]PCBM	190	0.75	11.9	0.67	6.0	2.4×10^{-3} [b]	-	107
P4, [70]PCBM	400	0.75	10.8	0.58	4.7	2.4×10^{-3} [b]	-	107
P5, [70]PCBM	250	0.88	12.4	0.71	7.7	4.3×10^{-3} [c]	-	108
P6, [70]PCBM	250	0.80	13.3	0.69	7.5	1.7×10^{-3} [a]	-	109
P7, [70]PCBM	108	0.78	15.4	0.69	8.3	6.7×10^{-2} [a]	-	110
P7, [70]PCBM	206	0.78	14.3	0.65	7.3	6.7×10^{-2} [a]	-	110
P8, [70]PCBM	100	0.85	13.3	0.68	7.7	9.3×10^{-2} [b]	-	51
P8, [70]PCBM	246	0.84	14.9	0.61	7.7	9.3×10^{-2} [b]	-	51
P9, [70]PCBM	290	0.79	16.3	0.73	9.4	3.0×10^{-3} [a]	1.5×10^{-3} [a]	111
P10, [70]PCBM	230	0.76	16.2	0.62	7.6	7.2×10^{-3} [a]	-	112
P11, [70]TCBM	300	0.75	18.8	0.75	10.8	1.7×10^{-2} [a]	-	27
P12, [70]TCBM	300	0.77	18.2	0.74	10.4	-	-	27

[a], SCLC mobility of polymer:fullerene blend film; [b], FET mobility of neat polymer film; [c], SCLC mobility of neat polymer film.

Attaching fluorine onto 2,1,3-benzothiadiazole (BT) leads to the generation of a family of photovoltaic polymers that outperform the polymers derived from BTA due to the extended spectral coverage in BT-based polymers. Wang et al.[110] synthesized a medium band gap polymer (P7) with BDT as donor unit and fluorinated BT as acceptor unit, which affords a PCE as high as 8.3% with a FF of 0.69 in BHJ solar cells at ≈110 nm active layer thickness. The increase of layer thickness to ≈210 nm results in a PCE of 7.3% due to a slight drop in FF and J_{sc}. The blend of P7:[70]PCBM exhibits notable hole mobility of 6.7×10^{-2} cm^{-2} V^{-1} s^{-1} as measured by SCLC method. Recently, Duan et al.[51] reported another high-performance polymer based on BDT and fluorinated BT, P8, which shows impressive efficiencies in a broad range of active layer thickness with a maximum PCE of 7.7% at active layer thickness of ≈100 and ≈250 nm, respectively. The importance of thick-film materials for tandem OSCs was highlighted in this work as the best tandem cells were fabricated at a relative high layer thickness of 155 nm for front subcell. Combining dialkoxyphenylene and fluorinated BT generates a semicrystalline medium band gap polymer, P9, which shows remarkable high PCE of up to 9.4% in a 290 nm thick BHJ solar cell.[111] The BHJ solar cells afford a high FF of 0.73 and EQE over 80% in the absorption range of 470–550 nm benefiting mainly from the efficient and balanced charge carrier transport. The average hole and electron mobilities in single-carrier diodes were estimated to be 3.0×10^{-3}, 1.5×10^{-3} cm^{-2} V^{-1} s^{-1}, respectively. Chen et al.[112] synthesized a D–A conjugated polymer P10 based on quarterthiophene and

fluorinated BT. The polymer shows very strong interchain aggregation in a room temperature solution, with an almost comparable absorption spectrum to that of the thin film. It is disclosed that such aggregation behavior has significant influence on polymer chain organization in solid state with a very high hole mobility of 1.92 cm^{-2} V^{-1} s^{-1} was observed in FET. It is worth noting that the SCLC mobility of P10:[70]PCBM is 7.2 × 10^{-3} cm^{-2} V^{-1} s^{-1}, which is at the same order of magnitude as the other thick-film polymers. BHJ solar cells with inverted device configuration at the active layer thickness range from 100 to 400 nm exhibited PCEs over 6.5%, whose maximum of 7.6% was realized at 230 nm thickness. By slightly shortening the alkyl chain on P10, a state-of-the-art polymer P11 was created by Yan's group.[27] The exquisite control of aggregation resulted in an unprecedented PCE of 10.8% and impressive FF of 0.75 in single junction BHJ solar cells based on P11 at an active layer thickness of 300 nm. As shown in Fig. 6, the EQE of the thick-film device exceeds 80% in a broad spectral range of 400–750 nm, representing around 20% enhancement with respect to the thin-film device. Moreover, the effective absorption bandwidth of a thick cell can be increased as the result of a ≈20 nm red-shift of the "leading, low energy edge" of a OSC's EQE spectrum. Combined, these account for a ≈30% enhancement in J_{sc}, clearly validating the benefits of thick-film OSCs. Removing the fluorine atoms from the BT unit to donor unit gives rise to a structural analog polymer P12, which also produces highly efficient solar cells with PCE of 10.4% and FF of 0.74 achieved at layer thickness of ≈300 nm.[27]

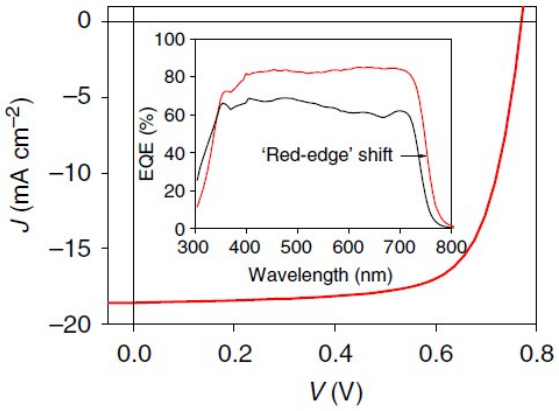

Fig. 6 Current density–voltage (*J*–*V*) curve of a P11:[70]PCBM cell under AM 1.5G illumination with an irradiation intensity of 100 mW cm^{-2}. Inset: representative EQE spectra of BHJ solar cells with a thick (300 nm) and thin (150 nm) active layer. The arrow indicates the shift of the "low energy edge" of the solar cells. Produced with the permission from ref. 27, Copyright 2014, Macmillan Publishers Limited.

3.3 Tetracyclic fused ring-based polymers

Conjugated polymers based on tetracyclic fused ring (e.g. naphtho[1,2-*c*:5,6-*c*]bis[1,2,5]-thiadiazole (NT)) also show attractive performance in thick-film BHJ solar cells benefiting from the large planar structure of tetracyclic fused ring, which can facilitate the interchain packing of the resulting polymers and enhance charge carrier mobility. The chemical structure of some tetracyclic fused ring-based polymers are shown in Scheme 3. Huang's group pioneered the development of NT-based semiconducting conjugated polymer for BHJ solar cells.[113-120] Impressively, P13, a polymer based on NT and BDT, shows PCE of 8.4% and FF of 0.61 at the active layer thickness of 250 nm in BHJ solar cells with inverted

device architecture.[114] Notably, the hole mobilities of P13 neat films were measured to be in the order of magnitude of 10^{-5} cm^{-2} V^{-1} s^{-1} in single-carrier devices. More interestingly, the hole mobility is dependent on the thickness of polymer films.[113] However, the SCLC hole mobility was measured to be 1.1×10^{-3} cm^{-2} V^{-1} s^{-1} in P13:[70]PCBM blend film, suggesting a large difference from that measured in pristine polymer. Through further contact optimization and morphology control, BHJ solar cells of P13:[70]PCBM yield PCE of 8.6% and 7.2%, and FF of 0.66 and 0.60 at the active layer thickness of 280 nm and 940 nm, respectively.[116] P14, a copolymer comprising naphtho[1,2-*b*:5,6-*b*']dithiophene (NDT) and NT, exhibits excellent photovoltaic properties with a PCE of 8.2% and FF of 0.64 with active layer thickness of 300 nm in BHJ solar cells. It was found that the linear alkyl chains on NDT units play an important role on this remarkable device performance. The conjugated backbone of P14 shows the face-on orientation toward substrate, while the analog of P14 without alkyl chains on NDT adopts the edge on orientation. The face-on orientation of P14 can facilitate the out-of-plane charge transport and thereby render the BHJ solar cells performed well at high active layer thickness.[121] The two polymers, P15 and P16, comprising the same conjugated backbone (alternating quarterthiophene and NT) but different alkyl chains, exhibit the unprecedented PCE of 10.1% with a FF of 0.68 and 0.73, respectively, in BHJ solar cells with active layer thickness of around 300 nm.[27] The high performance of P16 was attributed to the highly ordered polymer structure in the active layer, in which a highly crystalline structure with short π–π stacking distance and the favorable face-on orientation were achieved.[31] Kroon et

al.[122, 123] created a new tetracyclic fused ring building block and synthesized a new polymer, P17, which has a high band gap of 2.2 eV. Film microstructure studies revealed that P17 is semicrystalline and predominantly orders face-on in thin films, which persists upon blending with fullerenes. As a result, OSCs based on P17:fullerene blends produce high FF of >0.6 with regard to variations in active layer thickness up to 400 nm. Correspondingly, PCE of approximate 4% can be kept in a wide range of active layer thickness despite the absolute PCE value is not impressive owing to the narrow spectral response range.

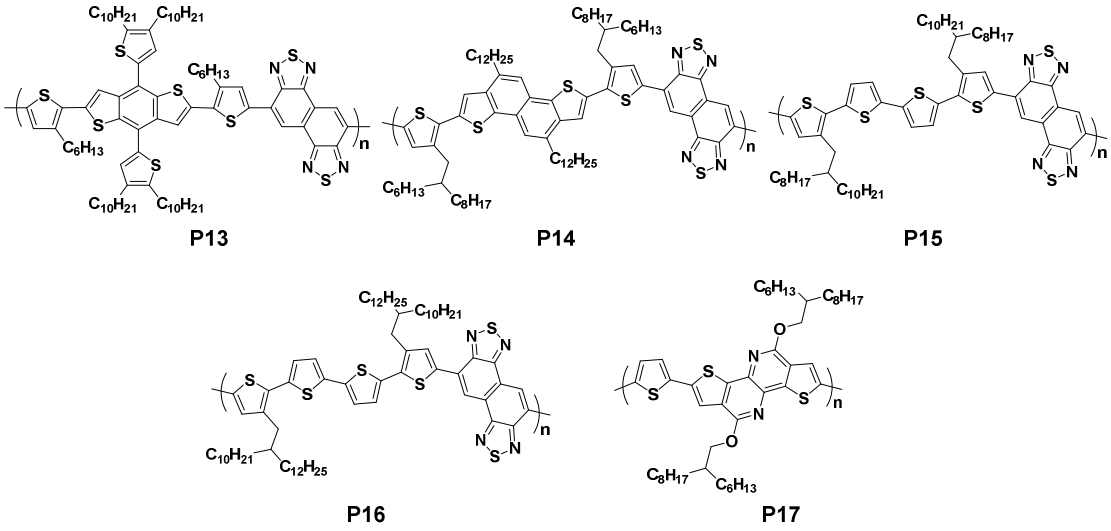

Scheme 3 The chemical structures of NT-based polymers that allow making efficient thick-film solar cells.

Table 3 BHJ solar cell performances of tetracyclic fused ring-based polymers that allow making efficient thick-film solar cells.

Polymer, acceptor	d (nm)	V_{oc} (V)	J_{sc} (mAcm^{-2})	FF (-)	PCE (%)	μ_h (cm^2 V^{-1} s^{-1})	μ_e (cm^2 V^{-1} s^{-1})	Ref.
P13, [70]PCBM	~90	0.80	11.7	0.61	6.0	10^{-5} [a]	-	113
P13, [70]PCBM	250	0.75	17.4	0.61	8.4	-	-	114
P13, [70]PCBM	280	0.74	17.6	0.66	8.6	1.1×10^{-3} [b]	-	116
P13, [70]PCBM	940	0.73	16.7	0.60	7.2	1.1×10^{-3} [b]	-	116
P14, [70]PCBM	300	0.82	15.6	0.64	8.2	3.0×10^{-3} [b]	-	121
P15, [70]PCBM	~300	0.76	19.8	0.68	10.1	-	-	27
P16, [70]PCBM	290	0.71	19.4	0.73	10.1	3.4×10^{-3} [b]	1.1×10^{-3} [b]	31
P17, [70]PCBM	~234	0.91	7.0	0.66	4.2	~3.0×10^{-3} [c]	-	122
P17, [70]PCBM	~315	0.91	7.9	0.63	4.6	~3.0×10^{-3} [c]	-	122
P17, [70]PCBM	~395	0.87	8.1	0.55	3.9	~3.0×10^{-3} [c]	-	122

[a], SCLC mobility of neat polymer film; [b], SCLC mobility of polymer:fullerene blend film; [c], FET mobility of neat polymer film.

3.4 Thiazole-derived polymers

Several thiazole-derived conjugated polymers (Scheme 4) show high FF and PCEs at relative high active layer thickness in BHJ solar cells. Peet et al.[124] reported a copolymer, P18, containing dithieno[3,2-b:2',3'-d]silole and thiazolothiazole, which shows best device performance at ≈170 nm thickness of active layer with FF of 0.66 and PCE of 4.7%. Further increasing the active layer thickness to ≈400 nm, a high FF exceeding 0.65 can be kept in the BHJ solar cells. Osaka et al.[125] developed a series of copolymers based on thiophene and thiazolothiazole with different side chain composition to systematically investigate the influence of side chain composition on the backbone orientation. It was disclosed that the BHJ solar cells using the polymers

with primary face-on orientation afforded high J_{sc} with thicker active layers without a loss of FF, while the cells using the polymers with edge-on or bimodal orientation gave a significant drop in FF and PCE. P19, a polymer with the well-ordered face-on orientation, affords maximum PCE of 7.5% and FF of 0.65 with the active layer thickness of 330 nm, and a PCE of close to 6% with thick layers of up to 1000 nm. Saeki et al.[126, 127] reported a benzobisthiazole and BT alternating copolymer, P20, in which benzobisthiazole serves as a weak donor unit rather than an acceptor unit. The BHJ solar cells with inverted device configuration based on P20 can afford a high FF of 0.67 and a PCE of 6.5% with active layer thickness of 210 nm. However, further increasing the layers thickness to 310 nm and 760 nm resulted in reduced FF of 0.6 and 0.55, respectively.

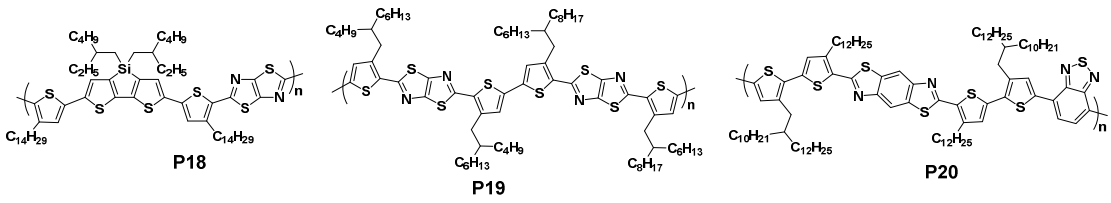

Scheme 4 The chemical structures of thiazole-derived polymers that allow making efficient thick-film solar cells.

Table 4 BHJ solar cell performances of thiazole-derived polymers that allow making efficient thick-film solar cells.

Polymer, acceptor	d (nm)	V_{oc} (V)	J_{sc} (mAcm^{-2})	FF (-)	PCE (%)	μ_h (cm^2 V^{-1} s^{-1})	μ_e (cm^2 V^{-1} s^{-1})	Ref.
P18, [60]PCBM	170	0.60	11.8	0.66	4.7	1.0×10^{-2} [a]	-	124
P19, [70]PCBM	330	0.90	12.7	0.65	7.5	4.8×10^{-4} [b]	-	125
P19, [60]PCBM	1020	0.87	12.9	0.51	5.8	4.8×10^{-4} [b]	-	125
P20, [70]PCBM	210	0.80	12.4	0.67	6.5	-	-	127
P20, [70]PCBM	310	0.78	12.3	0.60	5.5	-	-	127
P20, [70]PCBM	760	0.78	11.6	0.55	4.7	-	-	127

[a], FET mobility of neat polymer film; [b], SCLC mobility of polymer:fullerene blend film.

3.5 TPD-based polymers and analogs

Among a large number of conjugated polymers based on thieno[3,4-*c*]pyrrole-4,6-dione (TPD), a few of them exhibited high FF and PCE in thick-film BHJ solar cells. The chemical structures of these polymers are shown in Scheme 5 and the device results are summarized in Table 5. Guo et al.[128] synthesized a TPD-based polymer P21 and a structurally relevant polymer P22, which exhibited remarkable high FF of 0.76–0.80 in the BHJ solar cells with the active layer thickness of ≈120 nm. Impressively, a FF of >0.7 can be also obtained for the solar cells based on P21 even increasing the layer thickness to 300 nm, while the FF of P22-based devices decreased to 0.64 and 0.58 at active layer thickness of 200 nm and 270 nm, respectively. The unprecedented high FFs of P21- and P22-based solar cells were attributed to three aspects: 1) well-ordered face-on orientation toward electrode with close π–π interplanar spacing for high mobility; 2) ordered BHJ bicontinuous

networks for reduced charge trapping; and 3) preferential vertical phase gradation in inverted solar cells for suppressed charge carrier recombination.[128] The mapping of vertical phase gradation in the inverted OSCs based on P22:[70]PCBM blend film was established with the results from several complementary experimental techniques including cross-sectional transmission electron microscopy (TEM), energy-dispersive X-ray spectroscopy (EDS), and depth-profiled X-ray photoelectron spectroscopy (XPS). As shown in Fig. 7, optimal vertical phase gradation with polymer enrichment at the active layer/air interface, and [70]PCBM enrichment at the active layer/ZnO interface was formed in P22:[70]PCBM blend film. Such a vertical phase gradation is helpful to suppress electron leakage to the hole-collecting electrode and hole leakage to the electron-collecting electrode, thereby reducing recombination at the contacts and increasing FF.[128] Zhu et al.[129] reported a conjugated polymer based on zigzag naphthodithiophene and TPD, P23, that shows maximum PCE of 7.5% and a FF of 0.68 in BHJ solar cells with active layer thickness of ≈200 nm. At the active layer thickness range of 140–270 nm, the FF can be kept over 0.6. Interestingly, the analog of P23 having decyl on the bridging thiophene outward TPD unit shows significant FF drop with increasing layer thickness in solar cells. Recently, Jung et al.[130] developed a highly crystalline polymer P24 derived from TPD, which exhibits outstanding hole mobility of 1.9 cm^2 V^{-1} s^{-1} in FET. BHJ solar cells based on P24 show PCE of 7.1% and FF of 0.63 at the active layer thickness of 250 nm. Increasing the layer thickness to 450 nm, the PCE remains at >6% but the FF drops to 0.52. It was disclosed that the vinylene group in P24 plays an important role in intermolecular

interaction, well-ordered film microstructure, and charge carrier mobility as compared to the reference polymer without a vinylene bridge.

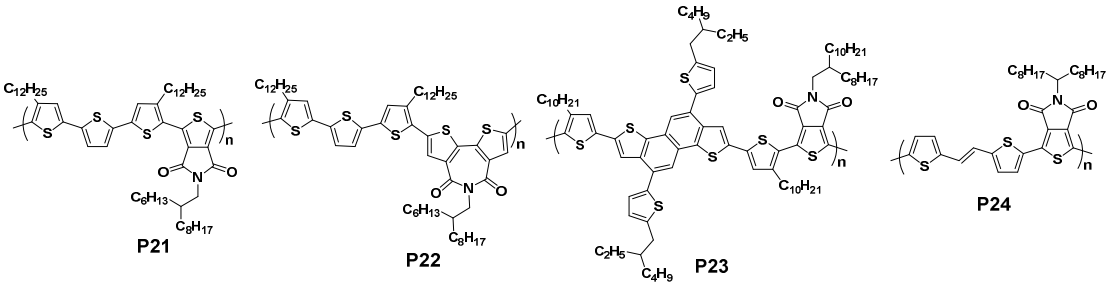

Scheme 5 The chemical structures of TPD-based polymers and analogs that allow making efficient thick-film solar cells.

Table 5 BHJ solar cell performances of TPD-based polymers and analogs that allow making efficient thick-film solar cells.

Polymer, acceptor	*d* (nm)	V_{oc} (V)	J_{sc} (mAcm^{-2})	FF (-)	PCE (%)	μ_h (cm^2 V^{-1} s^{-1})	μ_e (cm^2 V^{-1} s^{-1})	Ref.
P21, [70]PCBM	130	0.79	12.3	0.79	7.7	1.2×10^{-3} [a]	2.8×10^{-5} [b]	128
P21, [70]PCBM	300	0.75	12.1	0.71	6.4	1.2×10^{-3} [a]	2.8×10^{-5} [b]	128
P22, [70]PCBM	120	0.87	12.6	0.77	8.4	1.5×10^{-3} [a]	1.2×10^{-5} [b]	128
P22, [70]PCBM	200	0.84	11.5	0.64	6.2	1.5×10^{-3} [a]	1.2×10^{-5} [b]	128
P22, [70]PCBM	270	0.82	11.7	0.58	5.6	1.5×10^{-3} [a]	1.2×10^{-5} [b]	128
P23, [70]PCBM	203	0.86	12.7	0.68	7.5	1.1×10^{-3} [b]	-	129
P24, [70]PCBM	250	0.88	12.8	0.63	7.1	1.9 [c]	-	130
P24, [70]PCBM	450	0.87	13.8	0.52	6.2	1.9 [c]	-	130

[a], SCLC mobility of neat polymer; [b], SCLC mobility of polymer:fullerene blend film; [c], FET mobility of neat polymer film.

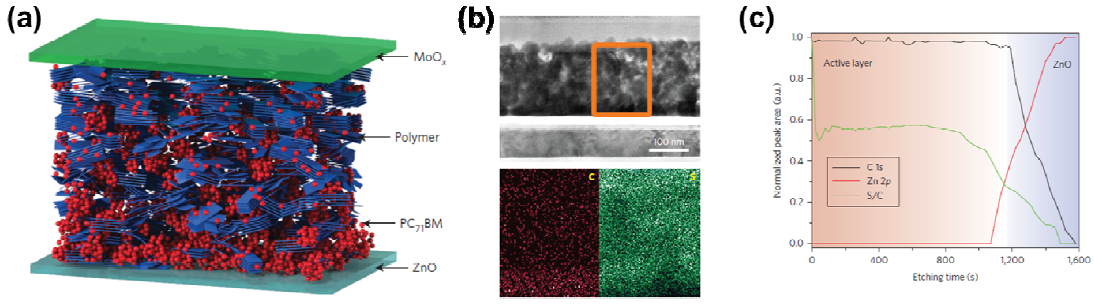

Fig. 7 Morphology of a P22:[70]PCBM film. (a) Schematic of the P22:[70]PCBM film showing vertical phase gradation with a polymer-rich layer near the MoO_x/blend interface and a [70]PCBM-rich layer near the blend/ZnO interface. (b) TEM cross-sectional image and EDS C and S mapping of an optimized P22:[70]PCBM inverted solar cells. (c) XPS depth profile of a P22:[70]PCBM blend film showing S:C ration evolution as a function of etching time, where etching begins at the air/film interface. Produced with permission from ref. 128, Copyright 2013, Macmillan Publishers Limited.

3.6 DPP-based polymers

Noticeably, the aforementioned polymers possessed relative large optical band gap (E_g), which are mostly larger than 1.6 eV. For the polymer with smaller E_g, achieving high FF and PCE at high active layer thickness is even challenging as the devices can generate more charge carriers due to increased light absorption and are thereby more susceptible to non-geminate recombination. The large planar aromatic lactam structure and strong electron-withdrawing ability of diketopyrrolopyrrole (DPP) usually render the resulting polymers very small optical band gap. Up to date, only a quite few DPP-based conjugated polymers perform well in BHJ solar cells with active

layer thickness over 200 nm. Li et al.[131] developed a high molecular weight polymer, P25, comprising DPP and thieno[3,2-*b*]thiophene, that has a high hole mobility of 0.8 cm^2 V^{-1} s^{-1} measured in FET and allows making efficient solar cells for thick active layers. The blend of P25 and [70]PCBM gives maximum PCE of 6.9% and a FF of 0.7 for film of 220 nm thickness. Further increasing the thickness to 300 nm, the BHJ solar cells can still show PCE of 6.3% with a FF of 0.61. More recently, Choi et al.[132] demonstrated an unprecedented J_{sc} of 20.1 mA cm^{-2}, a FF of 0.70, and a PCE of 9.4% for the BHJ solar cells based on P25 with active layer thickness of 340 nm through morphology engineering with optimal processing additive. The excellent device efficiency was attributed to the minimized recombination loss by bicontinuous interpenetrating network and high vertical charge carrier mobility as a result of close π-π face-on orientation. Recently, the use of P26, a polymer of the analog of P25 with different alkyl chains, enables making efficient large area solar cells (25 cm^2) with thick active layers. As shown in Fig. 8, The BHJ solar cells based on P26 with 250 nm film thickness afforded PCE of 6.2% and FF of 0.57 for 0.2 cm^2 device, PCE of 4.6% and FF of 0.53 for 25 cm^2 device.[46] Up to date, this is the highest PCE achieved in a large area monolithic architecture for OSCs. Gao et al.[133] discovered that alkyl chain geometry have significant influence on the pholotovoltaic properties of DPP polymers at high active layer thickness. By replacing the branched ethylhexyl group on the DPP unit with linear side chains, the structural order and charge carrier mobility of the modified polymers are enhanced. The polymers with linear side chains thus show slower PCE degradation than the polymer with branched chain when increasing the

thickness of active layer. For example, the BHJ solar cells based on P27 show PCE maximum of 6.9% and FF of 0.63 at 200 nm active layer thickness.[133]

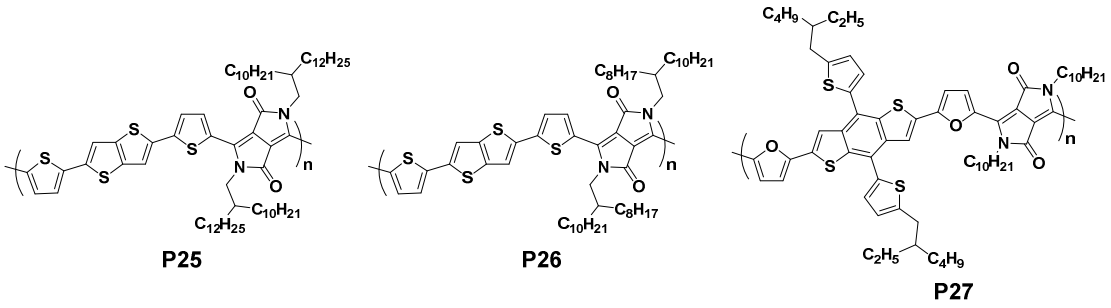

Scheme 6 The chemical structures of DPP-based polymers that allow making efficient thick-film solar cells.

Table 6 BHJ solar cell performances of DPP-based polymers that allow making efficient thick-film solar cells.

Polymer, acceptor	d (nm)	V_{oc} (V)	J_{sc} (mAcm^{-2})	FF (-)	PCE (%)	μ_h (cm^2 V^{-1} s^{-1})	μ_e (cm^2 V^{-1} s^{-1})	Ref.
P25, [70]PCBM	220	0.66	14.8	0.70	6.9	1.5 [a]	0.2 [a]	131
P25, [70]PCBM	300	0.67	15.5	0.61	6.3	1.5 [a]	0.2 [a]	131
P25, [70]PCBM	340	0.67	20.1	0.70	9.4	2.1×10^{-2} [b]	1.8×10^{-2} [b]	132
P26, [70]PCBM	250	0.67	17.0	0.57	6.2	1.5×10^{-3} [b]	2.0×10^{-3} [b]	46
P27, [70]PCBM	200	0.73	15.2	0.63	6.9	6.7×10^{-4} [b]	-	133

[a], FET mobility of neat polymer film; [b], SCLC mobility of polymer:fullerene blend film.

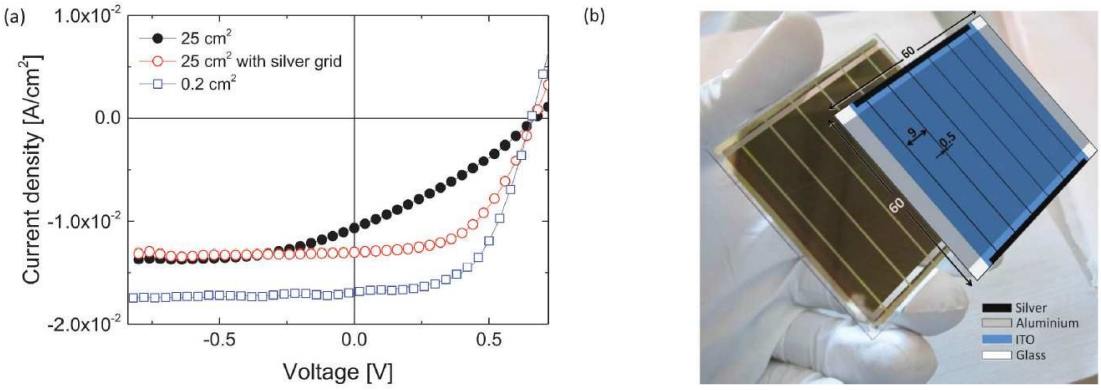

Fig. 8 (a) Current density–voltage (*J–V*) curves for thick (250 nm) large area monolithic solar cells based on P26:[70]PCBM under AM 1.5G illumination with and without a silver grid (best of three devices) compared with a small area device with the same active layer thickness and cell structure (representative *J–V* curve of at least six cells). (b) Photograph of a large area P26:[70]PCBM solar cell with transparent conducting electrode silver grid. The schematic of the device is also shown with approximate dimensions in mm. Produced with permission from ref. 46, Copyright 2015, John Wiley & Sons. Inc.

3.7 Small molecules

Although the state-of-the-art small molecule BHJ solar cells are comparable to polymer solar cells with PCE around 10% in single-junction devices,[32, 43] only two small molecular materials allow making efficient solar cells at active layer thickness over 200 nm. Sun et al.[134] reported a molecular donor material, S1, which exhibits unique nematic liquid behavior and excellent photovoltaic properties. The neat film of S1 showed hole mobility up to 0.1 $cm^2\ V^{-1}\ s^{-1}$ in FET, while the S1:[70]PCBM blend film supported a SCLC mobility of $1.6 \times 10^{-3}\ cm^2\ V^{-1}\ s^{-1}$. The BHJ solar cells based

on S1 and [70]PCBM demonstrated an impressive PCE of 9.3% with a high FF of 0.74 with active layer thickness of 250 nm. Thicker solar cells based on S1 with an active layer thickness up to 400 nm exhibited a PCE of 7.6% and a FF of 0.68. Another small molecule that allows making efficient thick-film solar cells is S2.[135] It was discovered that the concentration of solvent additive have significant influence on the solar cell performance when controlling the thickness of active layer via varying the concentration of S2:[70]PCBM blend. In brief, a constant mole fraction of solvent additive relative to the quantity of semiconducting material instead of host solvent volume is needed to obtain optimal active layer morphology and device performance at different active layer thickness. Through such an exquisite control of solvent additive concentration, a PCE of 5.7% and an

FF of 0.65 can be achieved in the S2:[70]PCBM solar cells with active layer thickness of ~200 nm.[136]

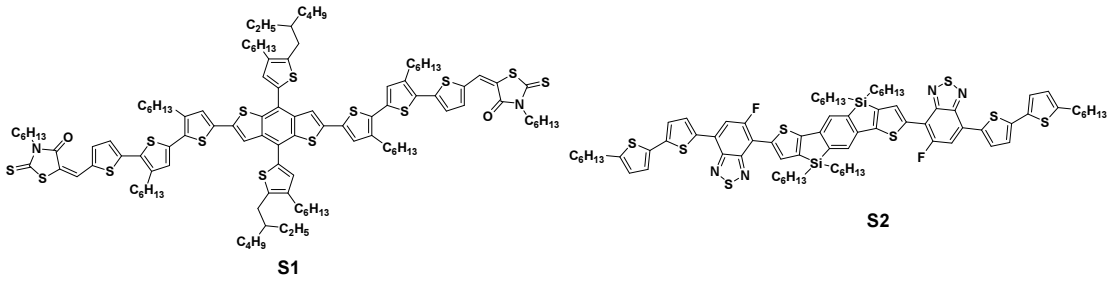

Scheme 7 The chemical structures of small molecules that allow making efficient thick-film solar cells.

Table 7 BHJ solar cell performances of small molecules that allow making efficient thick-film solar cells.

Polymer, acceptor	d (nm)	V_{oc} (V)	J_{sc} (mAcm^{-2})	FF (-)	PCE (%)	μ_h [a] (cm^2 V^{-1} s^{-1})	μ_e [a] (cm^2 V^{-1} s^{-1})	Ref.
S1, [70]PCBM	250	0.90	13.9	0.74	9.3	1.6×10^{-3}	9.6×10^{-3}	134
S1, [70]PCBM	400	0.88	12.7	0.68	7.6	1.6×10^{-3}	9.6×10^{-3}	134
S2, [70]PCBM	100	0.91	11.0	0.64	6.4	4.0×10^{-4}	1.0×10^{-3}	136
S2, [70]PCBM	200	0.88	9.9	0.65	5.7	4.0×10^{-4}	1.0×10^{-3}	136

[a], SCLC mobility of molecule:fullerene blend.

4. Conclusion and outlook

This review summarizes the progress of practically useful semiconducting conjugated polymers and small molecules, that are electron donors for making efficient thick-film BHJ solar cells. Despite a lot of conjugated polymers and small molecules show impressive high PCEs in single junction solar cells, most of these devices only perform well with a very small active layer thickness of around 80–120 nm, which is close to the first optical interference maxima. Further increasing the active layer thickness can improve the light absorption of the solar cells and are highly desirable for reproducibly manufacturing large-scale OSCs modules via high speed deposition methods such as roll-to-roll processing. However, increasing active layer thickness often results in worse overall device performance as a result of the sharp drop in FF and serious reduction of J_{sc} in most cases. Such an FF degradation in thick-film devices is the collective result of enhanced charge recombination due to lengthened

transport distance and the build-up of space-charge. Both effects are generally related to the low hole mobility of electron donors and the imbalanced charge transport inside the active layer. As discussed extensively above, several analysis have already highlighted the importance of high mobility and balance transport for achieving high FF in BHJ solar cells.

With the relative limited data acquired from reports, Fig. 9 shows a plot of SCLC hole mobilities measured in donor-acceptor blend films versus the FF of BHJ solar cells with active layer thickness in the range of 200–300 nm. As shown in Fig. 9. most data points with FF > 0.65 locate in the region with hole mobility $\geq 10^{-3}$ cm^2 V^{-1} s^{-1}. There are no data points with FF > 0.6 where the hole mobility is less than 4×10^{-4} cm^2 V^{-1} s^{-1}. This observation suggests that 10^{-3} cm^2 V^{-1} s^{-1} could be considered as a general mobility requirement for high FF in BHJ solar cells with active layer thickness over 200 nm. This threshold mobility and the general trend of mobility *vs.* FF are consistent with the result of drift-diffusion simulation.[59] Given the fact that electron mobility in BHJ solar cells can be relatively high ($\approx 5 \times 10^{-3}$ cm^{-2} V^{-1} s^{-1} measured by SCLC method)[72-74], the efforts should be placed on increasing the hole mobility of the electron donors in future.

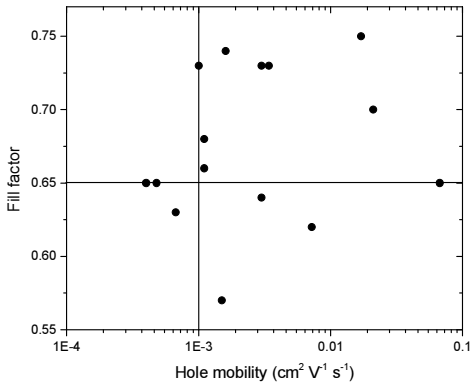

Fig. 9 Hole mobilities measured in blend films versus the FF of the corresponding BHJ solar cells with active layer thickness in the range of 200–300 nm.

Having established the importance of mobilities, we now consider lessons learned from the aforementioned donor materials about molecular design guidelines for high mobility donor materials. An important observation is that all materials possess rigid and planar backbones. The rigid coplanar structures are important because efficient intrachain charge-carrier transport rely on planar, straight polymer chains, while efficient interchain charge-carrier transport need closely π-stacked polymer aggregates.[59] The second observation is that the electron-donating segments in repeat units of the D-A type polymers are mostly no less than three elementary aromatic or heteroaromatic rings. The possible reason for this phenomenon is that big electron-rich segment would lead to large overlap of electron-rich segments between neighbouring polymer chains and thereby generate continuous channels for interchain hopping of charge carriers. Moreover, a lot of design rules for high mobility polymers in FETs have been established.[137-139] These lessons can also be borrowed for the design of new donor materials in thick BHJ solar cells. In addition, physical means

that can enhance hole mobilities also need to be investigated.

Introducing a highly crystalline conjugated polymer or small molecule with high mobility into the BHJ blend as the third component to form ternary blend may help to realize efficient thick-film OSCs. The highly crystalline third component may induce the crystallization and enhance molecular ordering in the donor phases. The formation of crystalline alloy structure can facilitate charge transport and suppress charge recombination. Several reports have already demonstrated the effectiveness of this strategy to improve the device performance in thin-film OSCs.[33, 140, 141] As pointed out by Bartelt et al.,[59] decreasing charge recombination rate, *k*, can reduce the mobility requirement for efficient thick-film OSCs. However, little is known about what factors affect *k* and how one can reduce *k* in a BHJ system. Bartelt et al.[59] have proposed several concepts such as spatially separating the holes and electrons in device, decreasing the density of charge-transfer states (CT-states) in the BHJ and slowing down CT-state recombination. Further research is needed to realize these concept in practical devices.

The film microstructure and BHJ morphology of the active layer dominate the performance of the OSCs. To realize efficient thick-film OSCs, more requirements are put forward for the film microstructure and BHJ morphology. In addition to bicontinuous interpenetrating network, high crystallinity and high degree of molecular ordering of the donor phases without increasing the domain size in BHJ films are needed to guarantee efficient exciton diffusion and charge transport. Pure phases are critical to suppress charge recombination and to afford a high FF at high active layer

thickness. Moreover, the molecular orientation have important influence on the performance of OSCs when the active layer becomes thick. As proved repeatedly in many cases, the face-on orientation is desired due to it is beneficial to vertical charge transport in OSCs.[80] The control of vertical phase gradation will also be highly fruitful as optimal vertical phase gradation can help to transport and to collect charges selectively at contacts. Up to date, the optimization of all of these metrics in a BHJ system is still highly challenging. With the synergistic progress in the development of new materials and the establishing of morphology manipulation methods toward efficient thick-film BHJ solar cells, we envision 15% PCE in single-junction devices and the industrialization of this advanced photovoltaic technology.

Acknowledgement

The work was financially supported by the Ministry of Science and Technology (No. 2014CB643501), the Natural Science Foundation of China (No. 21125419, 21490573 and 51361165301) and Guangdong Natural Science Foundation (Grant No. S2012030006232).

Reference

1. G. Yu, J. Gao, J. C. Hummelen, F. Wudl and A. J. Heeger, *Science*, 1995, **270**, 1789-1791.
2. L. Dou, J. You, Z. Hong, Z. Xu, G. Li, R. A. Street and Y. Yang, *Adv. Mater.*, 2013, **25**, 6642-6671.

3. C. J. Brabec, S. Gowrisanker, J. J. M. Halls, D. Laird, S. J. Jia and S. P. Williams, *Adv. Mater.*, 2010, **22**, 3839-3856.

4. F. C. Krebs, J. Fyenbo and M. Jorgensen, *J. Mater. Chem.*, 2010, **20**, 8994-9001.

5. L. Lu, T. Zheng, Q. Wu, A. M. Schneider, D. Zhao and L. Yu, *Chem. Rev.*, 2015, DOI: 10.1021/acs.chemrev.1025b00098.

6. J. Chen and Y. Cao, *Acc. Chem. Res.*, 2009, **42**, 1709-1718.

7. C. H. Duan, F. Huang and Y. Cao, *J. Mater. Chem.*, 2012, **22**, 10416-10434.

8. H. X. Zhou, L. Q. Yang and W. You, *Macromolecules*, 2012, **45**, 607-632.

9. Y. Li, *Acc. Chem. Res.*, 2012, **45**, 723-733.

10. L. Ye, S. Zhang, L. Huo, M. Zhang and J. Hou, *Acc. Chem. Res.*, 2014, **47**, 1595-1603.

11. Y. Y. Liang and L. P. Yu, *Acc. Chem. Res.*, 2010, **43**, 1227-1236.

12. Y. Chen, X. Wan and G. Long, *Acc. Chem. Res.*, 2013, **46**, 2645-2655.

13. E. Wang, W. Mammo and M. R. Andersson, *Adv. Mater.*, 2014, **26**, 1801-1826.

14. J. E. Coughlin, Z. B. Henson, G. C. Welch and G. C. Bazan, *Acc. Chem. Res.*, 2014, **47**, 257-270.

15. F. Liu, Y. Gu, J. W. Jung, W. H. Jo and T. P. Russell, *J. Polym. Sci. Part B: Polym. Phys.*, 2012, **50**, 1018-1044.

16. F. Liu, Y. Gu, X. Shen, S. Ferdous, H.-W. Wang and T. P. Russell, *Prog. Polym. Sci.*, 2013, **38**, 1990-2052.

17. Y. Huang, E. J. Kramer, A. J. Heeger and G. C. Bazan, *Chem. Rev.*, 2014, **114**,

7006-7043.

18. S. Kouijzer, J. J. Michels, M. van den Berg, V. S. Gevaerts, M. Turbiez, M. M. Wienk and R. A. J. Janssen, *J. Am. Chem. Soc.*, 2013, **135**, 12057-12067.

19. J. J. van Franeker, M. Turbiez, W. Li, M. M. Wienk and R. A. J. Janssen, *Nat. Commun.*, 2015, **6**, 6229.

20. C. Duan, K. Zhang, C. Zhong, F. Huang and Y. Cao, *Chem. Soc. Rev.*, 2013, **42**, 9071-9104.

21. H.-L. Yip and A. K. Y. Jen, *Energy Environ. Sci.*, 2012, **5**, 5994-6011.

22. S. K. Hau, H. L. Yip and A. K. Y. Jen, *Polymer Reviews*, 2010, **50**, 474-510.

23. O. Inganäs, F. Zhang, K. Tvingstedt, L. M. Andersson, S. Hellström and M. R. Andersson, *Adv. Mater.*, 2010, **22**, E100-E116.

24. T. Ameri, G. Dennler, C. Lungenschmied and C. J. Brabec, *Energy Environ. Sci.*, 2009, **2**, 347-363.

25. W. Li, A. Furlan, K. H. Hendriks, M. M. Wienk and R. A. J. Janssen, *J. Am. Chem. Soc.*, 2013, **135**, 5529-5532.

26. S.-H. Liao, H.-J. Jhuo, P.-N. Yeh, Y.-S. Cheng, Y.-L. Li, Y.-H. Lee, S. Sharma and S.-A. Chen, *Sci. Rep.*, 2014, **4**, 6813.

27. Y. Liu, J. Zhao, Z. Li, C. Mu, W. Ma, H. Hu, K. Jiang, H. Lin, H. Ade and H. Yan, *Nat. Commun.*, 2014, **5**, 5293.

28. J.-D. Chen, C. Cui, Y.-Q. Li, L. Zhou, Q.-D. Ou, C. Li, Y. Li and J.-X. Tang, *Adv. Mater.*, 2015, **27**, 1035-1041.

29. S. Zhang, L. Ye, W. Zhao, B. Yang, Q. Wang and J. Hou, *Sci. China Chem.*,

2015, **58**, 248-256.

30. Z. He, B. Xiao, F. Liu, H. Wu, Y. Yang, S. Xiao, C. Wang, T. P. Russell and Y. Cao, *Nat. Photonics*, 2015, **9**, 174-179.

31. V. Vohra, K. Kawashima, T. Kakara, T. Koganezawa, I. Osaka, K. Takimiya and H. Murata, *Nat. Photonics*, 2015, **9**, 403-408.

32. B. Kan, M. Li, Q. Zhang, F. Liu, X. Wan, Y. Wang, W. Ni, G. Long, X. Yang, H. Feng, Y. Zuo, M. Zhang, F. Huang, Y. Cao, T. P. Russell and Y. Chen, *J. Am. Chem. Soc.*, 2015, **137**, 3886-3893.

33. J. Zhang, Y. Zhang, J. Fang, K. Lu, Z. Wang, W. Ma and Z. Wei, *J. Am. Chem. Soc.*, 2015, **137**, 8176-8183.

34. C.-C. Chen, W.-H. Chang, K. Yoshimura, K. Ohya, J. You, J. Gao, Z. Hong and Y. Yang, *Adv. Mater.*, 2014, **26**, 5670-5677.

35. A. R. b. M. Yusoff, D. Kim, H. P. Kim, F. K. Shneider, W. J. da Silva and J. Jang, *Energy Environ. Sci.*, 2015, **8**, 303-316.

36. C. H. Peters, I. T. Sachs-Quintana, J. P. Kastrop, S. Beaupré, M. Leclerc and M. D. McGehee, *Adv. Energy Mater.*, 2011, **1**, 491-494.

37. M. Jørgensen, K. Norrman, S. A. Gevorgyan, T. Tromholt, B. Andreasen and F. C. Krebs, *Adv. Mater.*, 2012, **24**, 580-612.

38. Y. Liang, Z. Xu, J. Xia, S.-T. Tsai, Y. Wu, G. Li, C. Ray and L. Yu, *Adv. Mater.*, 2010, **22**, E135-E138.

39. L. Ye, S. Zhang, W. Zhao, H. Yao and J. Hou, *Chem. Mater.*, 2014, **26**, 3603-3605.

40. H.-Y. Chen, J. Hou, S. Zhang, Y. Liang, G. Yang, Y. Yang, L. Yu, Y. Wu and G. Li, *Nat. Photonics*, 2009, **3**, 649-653.

41. Y. I. H. Chao, J.-F. Jheng, J.-S. Wu, K.-Y. Wu, H.-H. Peng, M.-C. Tsai, C.-L. Wang, Y.-N. Hsiao, C.-L. Wang, C.-Y. Lin and C.-S. Hsu, *Adv. Mater.*, 2014, **26**, 5205-5210.

42. C. Cabanetos, A. El Labban, J. A. Bartelt, J. D. Douglas, W. R. Mateker, J. M. J. Fréchet, M. D. McGehee and P. M. Beaujuge, *J. Am. Chem. Soc.*, 2013, **135**, 4656-4659.

43. B. Kan, Q. Zhang, M. Li, X. Wan, W. Ni, G. Long, Y. Wang, X. Yang, H. Feng and Y. Chen, *J. Am. Chem. Soc.*, 2014, **136**, 15529-15532.

44. L. Dou, C.-C. Chen, K. Yoshimura, K. Ohya, W.-H. Chang, J. Gao, Y. Liu, E. Richard and Y. Yang, *Macromolecules*, 2013, **46**, 3384-3390.

45. R. S. Ashraf, I. Meager, M. Nikolka, M. Kirkus, M. Planells, B. C. Schroeder, S. Holliday, M. Hurhangee, C. B. Nielsen, H. Sirringhaus and I. McCulloch, *J. Am. Chem. Soc.*, 2014.

46. A. Armin, M. Hambsch, P. Wolfer, H. Jin, J. Li, Z. Shi, P. L. Burn and P. Meredith, *Adv. Energy Mater.*, 2015, **5**, 1401221.

47. J. Agostinelli, M. Kowarz and L. S. Liao, (Eastman Kodak), *US20060091794 A1*, 2004.

48. A. Armin, M. Hambsch, I. K. Kim, P. L. Burn, P. Meredith and E. B. Namdas, *Laser Photon. Rev.*, 2014, **8**, 924-932.

49. R. Søndergaard, M. Hösel, D. Angmo, T. T. Larsen-Olsen and F. C. Krebs,

Mater. Today, 2012, **15**, 36-49.

50. L. Dou, J. You, J. Yang, C.-C. Chen, Y. He, S. Murase, T. Moriarty, K. Emery, G. Li and Y. Yang, *Nat. Photonics*, 2012, **6**, 180-185.

51. C. Duan, A. Furlan, J. J. van Franeker, R. E. M. Willems, M. M. Wienk and R. A. J. Janssen, *Adv. Mater.*, 2015, **27**, 4461-4468.

52. T. Kirchartz, T. Agostinelli, M. Campoy-Quiles, W. Gong and J. Nelson, *J. Phys. Chem. Lett.*, 2012, **3**, 3470-3475.

53. H. Hoppe, S. Shokhovets and G. Gobsch, *Phys. Status Solidi RRL*, 2007, **1**, R40-R42.

54. L. A. A. Pettersson, L. S. Roman and O. Inganäs, *J. Appl. Phys.*, 1999, **86**, 487-496.

55. G. Dennler, M. C. Scharber and C. J. Brabec, *Adv. Mater.*, 2009, **21**, 1323-1338.

56. S. H. Park, A. Roy, S. Beaupre, S. Cho, N. Coates, J. S. Moon, D. Moses, M. Leclerc, K. Lee and A. J. Heeger, *Nat. Photonics*, 2009, **3**, 297-303.

57. J. A. Bartelt, Z. M. Beiley, E. T. Hoke, W. R. Mateker, J. D. Douglas, B. A. Collins, J. R. Tumbleston, K. R. Graham, A. Amassian, H. Ade, J. M. J. Fréchet, M. F. Toney and M. D. McGehee, *Adv. Energy Mater.*, 2013, **3**, 364-374.

58. Q. Zhang, B. Kan, F. Liu, G. Long, X. Wan, X. Chen, Y. Zuo, W. Ni, H. Zhang, M. Li, Z. Hu, F. Huang, Y. Cao, Z. Liang, M. Zhang, T. P. Russell and Y. Chen, *Nat. Photonics*, 2015, **9**, 35-41.

59. J. A. Bartelt, D. Lam, T. M. Burke, S. M. Sweetnam and M. D. McGehee, *Adv. Energy Mater.*, 2015, **5**, 1500577.

60. K. Sakai and M. Hiramoto, *Mol. Cryst. Liq. Cryst.*, 2008, **491**, 284-289.

61. P. P. Boix, G. Garcia-Belmonte, U. Muñecas, M. Neophytou, C. Waldauf and R. Pacios, *Appl. Phys. Lett.*, 2009, **95**, 233302.

62. S. Khelifi, K. Decock, J. Lauwaert, H. Vrielinck, D. Spoltore, F. Piersimoni, J. Manca, A. Belghachi and M. Burgelman, *J. Appl. Phys.*, 2011, **110**, 094509.

63. W. Tress, K. Leo and M. Riede, *Phys. Rev. B*, 2012, **85**, 155201.

64. M. Morana, H. Azimi, G. Dennler, H.-J. Egelhaaf, M. Scharber, K. Forberich, J. Hauch, R. Gaudiana, D. Waller, Z. Zhu, K. Hingerl, S. S. van Bavel, J. Loos and C. J. Brabec, *Adv. Funct. Mater.*, 2010, **20**, 1180-1188.

65. M. C. Scharber, M. Koppe, J. Gao, F. Cordella, M. A. Loi, P. Denk, M. Morana, H.-J. Egelhaaf, K. Forberich, G. Dennler, R. Gaudiana, D. Waller, Z. Zhu, X. Shi and C. J. Brabec, *Adv. Mater.*, 2010, **22**, 367-370.

66. L. J. A. Koster, E. C. P. Smits, V. D. Mihailetchi and P. W. M. Blom, *Phys. Rev. B*, 2005, **72**, 085205.

67. R. Häusermann, E. Knapp, M. Moos, N. A. Reinke, T. Flatz and B. Ruhstaller, *J. Appl. Phys.*, 2009, **106**, 104507.

68. T. Kirchartz, B. E. Pieters, J. Kirkpatrick, U. Rau and J. Nelson, *Phys. Rev. B*, 2011, **83**, 115209.

69. W. Tress, K. Leo and M. Riede, *Adv. Funct. Mater.*, 2011, **21**, 2140-2149.

70. C. M. Proctor, J. A. Love and T.-Q. Nguyen, *Adv. Mater.*, 2014, **26**,

5957-5961.

71. A. Armin, G. Juska, M. Ullah, M. Velusamy, P. L. Burn, P. Meredith and A. Pivrikas, *Adv. Energy Mater.*, 2014, **4**, 1300954.

72. V. D. Mihailetchi, J. K. J. van Duren, P. W. M. Blom, J. C. Hummelen, R. A. J. Janssen, J. M. Kroon, M. T. Rispens, W. J. H. Verhees and M. M. Wienk, *Adv. Funct. Mater.*, 2003, **13**, 43-46.

73. V. D. Mihailetchi, H. X. Xie, B. de Boer, L. J. A. Koster and P. W. M. Blom, *Adv. Funct. Mater.*, 2006, **16**, 699-708.

74. A. C. Stuart, J. R. Tumbleston, H. Zhou, W. Li, S. Liu, H. Ade and W. You, *J. Am. Chem. Soc.*, 2013, **135**, 1806-1815.

75. L. Lu and L. Yu, *Adv. Mater.*, 2014, **26**, 4413-4430.

76. F. Liu, W. Zhao, J. R. Tumbleston, C. Wang, Y. Gu, D. Wang, A. L. Briseno, H. Ade and T. P. Russell, *Adv. Energy Mater.*, 2014, **4**, 1301377.

77. B. A. Collins, Z. Li, J. R. Tumbleston, E. Gann, C. R. McNeill and H. Ade, *Adv. Energy Mater.*, 2013, **3**, 65-74.

78. Y. Kim, S. Cook, S. M. Tuladhar, S. A. Choulis, J. Nelson, J. R. Durrant, D. D. C. Bradley, M. Giles, I. McCulloch, C. S. Ha and M. Ree, *Nat. Mater.*, 2006, **5**, 197-203.

79. S. Albrecht, J. R. Tumbleston, S. Janietz, I. Dumsch, S. Allard, U. Scherf, H. Ade and D. Neher, *J. Phys. Chem. Lett.*, 2014, **5**, 1131-1138.

80. I. Osaka and K. Takimiya, *Polymer*, 2015, **59**, A1-A15.

81. A. Claudia Arias, *J. Macromol. Sci. C*, 2006, **46**, 103-125.

82. L.-M. Chen, Z. Hong, G. Li and Y. Yang, *Adv. Mater.*, 2009, **21**, 1434-1449.

83. A. Tada, Y. Geng, Q. Wei, K. Hashimoto and K. Tajima, *Nat. Mater.*, 2011, **10**, 450-455.

84. Z. Xiao, Y. Yuan, B. Yang, J. VanDerslice, J. Chen, O. Dyck, G. Duscher and J. Huang, *Adv. Mater.*, 2014, **26**, 3068-3075.

85. J. Kong, I.-W. Hwang and K. Lee, *Adv. Mater.*, 2014, **26**, 6275-6283.

86. M. T. Dang, L. Hirsch and G. Wantz, *Adv. Mater.*, 2011, **23**, 3597-3602.

87. A. J. Moulé, J. B. Bonekamp and K. Meerholz, *J. Appl. Phys.*, 2006, **100**, 094503.

88. H. Jin, J. Olkkonen, M. Tuomikoski, P. Kopola, A. Maaninen and J. Hast, *Sol. Energy Mater. Sol. Cells*, 2010, **94**, 465-470.

89. P. Schilinsky, C. Waldauf and C. J. Brabec, *Appl. Phys. Lett.*, 2002, **81**, 3885-3887.

90. S. Lee, S. Nam, H. Kim and Y. Kim, *Appl. Phys. Lett.*, 2010, **97**, 103503.

91. L. Zeng, C. W. Tang and S. H. Chen, *Appl. Phys. Lett.*, 2010, **97**, 053305.

92. X. Guo, C. Cui, M. Zhang, L. Huo, Y. Huang, J. Hou and Y. Li, *Energy Environ. Sci.*, 2012, **5**, 7943-7949.

93. S. H. Liao, Y. L. Li, T. H. Jen, Y. S. Cheng and S. A. Chen, *J. Am. Chem. Soc.*, 2012, **134**, 14271-14274.

94. M. Zhang, X. Guo, W. Ma, H. Ade and J. Hou, *Adv. Mater.*, 2014, **26**, 5880-5885.

95. Z. Zheng, S. Zhang, M. Zhang, K. Zhao, L. Ye, Y. Chen, B. Yang and J. Hou,

Adv. Mater., 2015, **27**, 1189-1194.

96. Y. Liang, D. Feng, Y. Wu, S.-T. Tsai, G. Li, C. Ray and L. Yu, *J. Am. Chem. Soc.*, 2009, **131**, 7792-7799.

97. H. J. Son, W. Wang, T. Xu, Y. Liang, Y. Wu, G. Li and L. Yu, *J. Am. Chem. Soc.*, 133, **133**, 1885-1894.

98. B. C. Schroeder, Z. Huang, R. S. Ashraf, J. Smith, P. D'Angelo, S. E. Watkins, T. D. Anthopoulos, J. R. Durrant and I. McCulloch, *Adv. Funct. Mater.*, 2012, **22**, 1663-1670.

99. N. E. Jackson, B. M. Savoie, K. L. Kohlstedt, M. Olvera de la Cruz, G. C. Schatz, L. X. Chen and M. A. Ratner, *J. Am. Chem. Soc.*, 2013, **135**, 10475-10483.

100. C. B. Nielsen, A. J. P. White and I. McCulloch, *J. Org. Chem.*, 2015, **80**, 5045-5048.

101. J. R. Tumbleston, B. A. Collins, L. Yang, A. C. Stuart, E. Gann, W. Ma, W. You and H. Ade, *Nat. Photonics*, 2014, **8**, 385-391.

102. S. Albrecht, S. Janietz, W. Schindler, J. Frisch, J. Kurpiers, J. Kniepert, S. Inal, P. Pingel, K. Fostiropoulos, N. Koch and D. Neher, *J. Am. Chem. Soc.*, 2012, **134**, 14932-14944.

103. S. C. Price, A. C. Stuart, L. Q. Yang, H. X. Zhou and W. You, *J. Am. Chem. Soc.*, 2011, **133**, 4625-4631.

104. W. Li, L. Yang, J. R. Tumbleston, L. Yan, H. Ade and W. You, *Adv. Mater.*, 2014, **26**, 4456-4462.

105. W. Li, S. Albrecht, L. Yang, S. Roland, J. R. Tumbleston, T. McAfee, L. Yan, M. A. Kelly, H. Ade, D. Neher and W. You, *J. Am. Chem. Soc.*, 2014, **136**, 15566-15576.

106. J. R. Tumbleston, A. C. Stuart, E. Gann, W. You and H. Ade, *Adv. Funct. Mater.*, 2013, **23**, 3463-3470.

107. J. Min, Z.-G. Zhang, S. Zhang and Y. Li, *Chem. Mater.*, 2012, **24**, 3247-3254.

108. K. Li, Z. Li, K. Feng, X. Xu, L. Wang and Q. Peng, *J. Am. Chem. Soc.*, 2013, **135**, 13549-13557.

109. Z. Li, H. Lin, K. Jiang, J. Carpenter, Y. Li, Y. Liu, H. Hu, J. Zhao, W. Ma, H. Ade and H. Yan, *Nano Energy*, 2015, **15**, 607-615.

110. N. Wang, Z. Chen, W. Wei and Z. Jiang, *J. Am. Chem. Soc.*, 2013, **135**, 17060-17068.

111. T. L. Nguyen, H. Choi, S. J. Ko, M. A. Uddin, B. Walker, S. Yum, J. E. Jeong, M. H. Yun, T. J. Shin, S. Hwang, J. Y. Kim and H. Y. Woo, *Energy Environ. Sci.*, 2014, **7**, 3040-3051.

112. Z. Chen, P. Cai, J. Chen, X. Liu, L. Zhang, L. Lan, J. Peng, Y. Ma and Y. Cao, *Adv. Mater.*, 2014, **26**, 2586-2591.

113. M. Wang, X. W. Hu, P. Liu, W. Li, X. Gong, F. Huang and Y. Cao, *J. Am. Chem. Soc.*, 2011, **133**, 9638-9641.

114. T. Yang, M. Wang, C. Duan, X. Hu, L. Huang, J. Peng, F. Huang and X. Gong, *Energy Environ. Sci.*, 2012, **5**, 8208-8214.

115. M. Wang, X. Hu, L. Liu, C. Duan, P. Liu, L. Ying, F. Huang and Y. Cao,

Macromolecules, 2013, **46**, 3950-3958.

116. X. Hu, C. Yi, M. Wang, C.-H. Hsu, S. Liu, K. Zhang, C. Zhong, F. Huang, X. Gong and Y. Cao, *Adv. Energy Mater.*, 2014, **4**, 1400378.

117. L.-Q. Liu, G.-C. Zhang, P. Liu, J. Zhang, S. Dong, M. Wang, Y.-G. Ma, H.-L. Yip and F. Huang, *Chem. Asian J.*, 2014, **9**, 2104-2112.

118. W. Li, Q. Li, S. Liu, C. Duan, L. Ying, F. Huang and Y. Cao, *Sci. China Chem.*, 2015, **58**, 257-266.

119. L. Liu, G. Zhang, B. He and F. Huang, *Chin. J. Chem.*, 2015, **33**, 902-908.

120. P. Liu, S. Dong, F. Liu, X. Hu, L. Liu, Y. Jin, S. Liu, X. Gong, T. P. Russell, F. Huang and Y. Cao, *Adv. Funct. Mater.*, 2015, DOI: 10.1002/adfm.201501878.

121. I. Osaka, T. Kakara, N. Takemura, T. Koganezawa and K. Takimiya, *J. Am. Chem. Soc.*, 2013, **135**, 8834-8837.

122. R. Kroon, A. Diaz de Zerio Mendaza, S. Himmelberger, J. Bergqvist, O. Bäcke, G. C. Faria, F. Gao, A. Obaid, W. Zhuang, D. Gedefaw, E. Olsson, O. Inganäs, A. Salleo, C. Müller and M. R. Andersson, *J. Am. Chem. Soc.*, 2014, **136**, 11578-11581.

123. R. Kroon, A. Diaz de Zerio Mendaza, S. Himmelberger, J. Bergqvist, O. Bäcke, G. C. Faria, F. Gao, A. Obaid, W. Zhuang, D. Gedefaw, E. Olsson, O. Inganäs, A. Salleo, C. Müller and M. R. Andersson, *J. Am. Chem. Soc.*, 2015, **137**, 550-550.

124. J. Peet, L. Wen, P. Byrne, S. Rodman, K. Forberich, Y. Shao, N. Drolet, R. Gaudiana, G. Dennler and D. Waller, *Appl. Phys. Lett.*, 2011, **98**, 043301.

125. I. Osaka, M. Saito, T. Koganezawa and K. Takimiya, *Adv. Mater.*, 2014, **26**, 331-338.

126. M. Tsuji, A. Saeki, Y. Koizumi, N. Matsuyama, C. Vijayakumar and S. Seki, *Adv. Funct. Mater.*, 2014, **24**, 28-36.

127. A. Saeki, M. Tsuji, S. Yoshikawa, A. Gopal and S. Seki, *J. Mater. Chem. A*, 2014, **2**, 6075-6080.

128. X. Guo, N. Zhou, S. J. Lou, J. Smith, D. B. Tice, J. W. Hennek, R. P. Ortiz, J. T. L. Navarrete, S. Li, J. Strzalka, L. X. Chen, R. P. H. Chang, A. Facchetti and T. J. Marks, *Nat. Photonics*, 2013, **7**, 825-833.

129. X. Zhu, J. Fang, K. Lu, J. Zhang, L. Zhu, Y. Zhao, Z. Shuai and Z. Wei, *Chem. Mater.*, 2014, **26**, 6947-6954.

130. J. W. Jung, T. P. Russell and W. H. Jo, *ACS Appl. Mater. Interfaces*, 2015, **7**, 13666-13674.

131. W. Li, K. H. Hendriks, W. S. C. Roelofs, Y. Kim, M. M. Wienk and R. A. J. Janssen, *Adv. Mater.*, 2013, **25**, 3182-3186.

132. H. Choi, S.-J. Ko, T. Kim, P.-O. Morin, B. Walker, B. H. Lee, M. Leclerc, J. Y. Kim and A. J. Heeger, *Adv. Mater.*, 2015, **27**, 3318-3324.

133. J. Gao, L. Dou, W. Chen, C.-C. Chen, X. Guo, J. You, B. Bob, W.-H. Chang, J. Strzalka, C. Wang, G. Li and Y. Yang, *Adv. Energy Mater.*, 2014, **4**, 1300739.

134. K. Sun, Z. Xiao, S. Lu, W. Zajaczkowski, W. Pisula, E. Hanssen, J. M. White, R. M. Williamson, J. Subbiah, J. Ouyang, A. B. Holmes, W. W. H. Wong and D. J. Jones, *Nat. Commun.*, 2015, **6**, 6013.

135. J. A. Love, I. Nagao, Y. Huang, M. Kuik, V. Gupta, C. J. Takacs, J. E. Coughlin, L. Qi, T. S. van der Poll, E. J. Kramer, A. J. Heeger, T.-Q. Nguyen and G. C. Bazan, *J. Am. Chem. Soc.*, 2014, **136**, 3597-3606.

136. J. A. Love, S. D. Collins, I. Nagao, S. Mukherjee, H. Ade, G. C. Bazan and T.-Q. Nguyen, *Adv. Mater.*, 2014, **26**, 7308-7316.

137. P. M. Beaujuge and J. M. J. Fréchet, *J. Am. Chem. Soc.*, 2011, **133**, 20009-20029.

138. C. Wang, H. Dong, W. Hu, Y. Liu and D. Zhu, *Chem. Rev.*, 2012, **112**, 2208-2267.

139. J. Mei, Y. Diao, A. L. Appleton, L. Fang and Z. Bao, *J. Am. Chem. Soc.*, 2013, **135**, 6724-6746.

140. Y. Zhang, D. Deng, K. Lu, J. Zhang, B. Xia, Y. Zhao, J. Fang and Z. Wei, *Adv. Mater.*, 2015, **27**, 1071-1076.

141. S. Liu, P. You, J. Li, J. Li, C.-S. Lee, B. S. Ong, C. Surya and F. Yan, *Energy Environ. Sci.*, 2015, **8**, 1463-1470.

Table of Content for

Solution Processed Thick Film Organic Solar Cells

Chunhui Duan, Fei Huang,* Yong Cao

In this Review article, significant advances in materials development and processing methods toward efficient solution processed bulk-heterojunction thick film organic solar cells as well as the factors that determine the optimal active layer thickness are summarized.